UNIVERSIDAD MIGUEL HERNÁNDEZ DE ELCHE

FACULTAD DE MEDICINA

Departamento de Psicologia Clínica

Evaluación del protocolo óptimo de tomografía computarizada en pacientes con aneurismas o disecciones aórticas sometidos a tratamiento endovascular

SEGURIDAD DEL PACIENTE DESDE EL SERVICIO DE RADIOLOGIA

TESIS DOCTORAL

Modalidad de presentación de tesis doctoral con un conjunto de publicaciones

Presentada por:

LUCIA FLORS BLASCO

Dirigida por:

Dra. MARIA SALINAS LA CASTA

Dr. DOMINGO OROZCO BELTRAN

Prof. Dr. JOSE J. MIRA SOLBES

Alicante, Junio de 2014

UNIVERSITAS
Miguel
Hernández

"*Quality is the extent to which the right procedure is done in the right way at the right time, and the correct interpretation is accurately and quickly communicated to the patient and referring physician*."

Hillman, B.J.

To my beloved Carlos

To my parents

To my brother Carlos and my sister Carla

To my mentor KD Hagspiel

To those who fill my live with good moments

FACTOR DE IMPACTO DEL CONJUNTO DE PUBLICACIONES EN LAS QUE SE BASA LA PRESENTE TESIS DOCTORAL

1. Endoleak detection after endovascular repair of thoracic aortic aneurysm using dual-source dual-energy CT: suitable scanning protocols and potential radiation dose reduction. Flors L, Leiva-Salinas C, Norton PT, Patrie JT, Hagspiel KD. AJR Am J Roentgenol. 2013 Feb;200(2):451-60.

FACTOR DE IMPACTO 2,9 (Indexada en la base bibliométrica JCR (Journal Citation Report)

Categoría: RADIOLOGY, NUCLEAR MEDICINE AND MEDICAL IMAGING

Posición que ocupa la revista en la categoria: 28 de 120

2. Imaging Follow-up of Endovascular Repair of Type B Aortic Dissection with Dual-Source, Dual-Energy CT and Late Delayed-Phase Scans. Flors L, Leiva-Salinas C, Norton PT, Patrie JT, Hagspiel KD. J Vasc Interv Radiol. J **Vasc Interv Radiol. 2014 Mar;25(3):435-42.**

FACTOR DE IMPACTO: 2 (Indexada en la base bibliométrica JCR (Journal Citation Report)

Categoría: RADIOLOGY, NUCLEAR MEDICINE AND MEDICAL IMAGING

Posición que ocupa la revista en la categoria: 48 de 120

INDICE

INTRODUCCIÓN

1. INTRODUCCIÓN

1.1. Patient Safety

The delivery of safe, high-quality health care has always been a goal of physicians, nurses and other health-care professionals [1]. Evidence from many studies indicates that patients are being harmed while receiving health-care services, and the Institute of Medicine's report on medical errors published in 1999 [2] referenced studies that suggest that thousands of patients die each year in U.S. hospitals as a result of errors. An even larger number of patients are seriously harmed as a result of adverse events despite the best intentions of dedicated, hard-working health-care providers [1].

During the last several decades, extraordinary advances in technology in health care have led to a dramatic increase in complexity within the system. Physicians and nurses now have thousands of potent medications to administer to patients, specialists have highly complex and technologically advanced equipment to diagnose disease or deliver treatment, and all health-care professionals now have tremendous amounts of information available to them through websites and data repositories [1]. With all these advances and innovations, however, come more opportunities for error, unless there is an accompanying change in the infrastructure to manage the new levels of complexity [1].

1.2. Patient Safety in Radiology

1.2.1. Patient Safety in Radiology:Introduction

Advanced imaging technology, primarily cross-sectional imaging, is rapidly contributing to the transformation of healthcare worldwide. Along with advanced imaging modalities and their technical protocols come increased responsibilities for radiologists to meet.

There are multiple areas for potential error and resultant harm in radiology. Because the functions of radiology are primarily related to diagnosis, many errors in radiology departments can delay diagnosis and treatment. Such errors can result from mistaken identification of patients, failure to execute the technical aspects of image acquisition, lack or misperception of imaging findings, misinterpretation of identified imaging findings, and failure to effectively communicate imaging findings in an appropriate and timely manner to the person who needs that information to act (lost or unavailable images and reports or delayed communication of results) [3, 4]. Since procedures are often performed in radiology, errors also can be related to procedural complications or wrong sites of procedures, such as performing nephrostomy on the wrong side in a patient with bilateral hydronephrosis or performing.

Radiology presents multiple opportunities to improve the safety of patient care. Because radiologic care affects most inpatients and outpatients at a medical center, the impact of safety improvement is potentially large, particularly in interventional procedures, examinations involving radiation exposure, and drug administration [5]. Because the potential for harm in radiology departments is high, the opportunities to provide safer care are great [5].

1.2.2. Quality and Safety Programs in Radiology

To ensure safety, accuracy, and high-quality care and to allow radiologists and radiology personnel to maintain a competitive edge in an increasingly complex environment, it is essential that all imaging departments establish and maintain managed, comprehensive, and effective performance improvement programs [6].

The structure and components of a departmental performance improvement program vary depending on the size of the department and hospital, the nature of the practice and the services offered, and the institutional mission and culture of quality and safety [6]. Basic components include patient safety, process improvement, customer service, professional staff assessment, and education, each of which requires strategies for implementing continuous programs to monitor performance, analyzing and depicting data, implementing change, and meeting regulatory requirements [6].

Hillman et al [7] provided an excellent definition of Quality in Radiology: "*Quality is the extent to which the right procedure is done in the right way at the right time, and the correct interpretation is accurately and quickly communicated to the patient and referring physician*."

The key components of quality in radiology are: 1) appropriateness of the examination; 2) the procedure protocol; 3) accuracy of interpretation, 4) communication of results, and 5) measuring and monitoring performance improvement in quality, safety, and efficiency [8].

Appropriateness of the examination is represented by the term *the right procedure* [7, 8]. There are two aspects: appropriateness of the examination requested by the referring physician and appropriateness of the examination performed (the imaging protocol). Radiologists and referring physicians must be knowledgeable about which imaging procedure is appropriate for each clinical indication.

In the definition of quality, the procedure protocol is represented by the term *the right way*. Once the correct procedure is requested, the correct protocol for the procedure must be selected and communicated to the technologist who will perform the study [7, 8].

Accuracy of interpretation is represented by the term *the correct interpretation*. Once the imaging procedure has been performed, the radiologist reviews the images. The radiologist's task is to accurately perceive and interpret the imaging observations (radiologic diagnosis) [7, 8].

Communication of results is represented by the phrase *accurately and quickly communicated*. Once the radiologist provides an interpretation and recommendation, those results must be communicated to the referring physician and the patient in a timely manner, depending on the type of result (ie, critical results vs noncritical results) [7, 8].

Finally, measuring and monitoring performance improvement in quality, safety, and efficiency is represented by the phrase *patient and referring physician*. Ultimately, the effectiveness of radiology is judged by the accuracy of radiologist performance, efficient service, and avoidance of unintended patient

complications.

1.2.3. Safety Metrics Relevant to Radiology

Radiologists and institutions must measure and monitor indicators of quality, safety, and efficiency in their services to prove that imaging and their interventions are of high quality [7, 8].These aspects of quality arise directly out of the sequence of events that make up the healthcare process in radiology. It is understood as the "value map" for radiology because it specifies each of the steps that can go wrong during the care of the patient. Consequently, each of these steps should be part of a quality assurance program (Table 1).

Table 1: Sequence of Events in the Radiology Care Process (Adapted from Rubin DL[8]

Event	Metrics
Referring physician orders a radiological exam	• Appropriateness guidelines (ordering error)
Appointment scheduled	• Access times
Initial radiology encounter	• Patient wait time • Patient instructions and preparation
Protocol selection	• Standardized protocol

Patient examination	• Environment of care, safety, and comfort • Procedural complications
Interpretation of the exam	• Correct subspecialty interpretation • Accuracy • Structured report • Report answers clinical question
Finalization errors	• Timelines • Succinctness
Communication (emergent or important)	• Referring physician satisfaction • Query answered or addressed
Measuring and monitoring performance improvement in quality, safety, and efficiency	• Turnaround time in examinations and reporting • Rate of overreading agreement • Patient complications • Patient satisfaction

1.2.4. Strategies and Culture Transformation

Vertically oriented interventions are aimed at a specific process, technology, or related areas of error, typically a specific process in which errors have been historically common. Horizontally oriented interventions are aimed at improving the culture or environment of the department in an effort to reduce the number of human errors potentially leading to patient harm. Both types of intervention are needed to establish a comprehensive safety program for improving safety performance in radiology [4].

Historically, radiology has been a leader in instigating vertically, or tactically, oriented initiatives for addressing specific safety issues. Examples include efforts at dose reduction for pediatric CT, minimization of contrast-induced nephropathy, and optimal response to allergic reactions to contrast material, MRI safety, and implementation of information systems for optimal triage and communication of results. Few publications, however, describe implementation of horizontal interventions to change culture and behavior to minimize the number of human errors occurring in radiology departments [4].

The key to improving patient safety lies in changing the culture from one of blame and shame to one in which health-care professionals acknowledge the ubiquity of risk and take responsibility for reducing risk—one in which health-care providers acknowledge the complexity of care and recognize errors as opportunities to learn and to reduce risk. In order to create a culture of safety, hospitals and institutions must create a non-punitive environment for reporting and facilitate learning by providing opportunities for health-care providers to share stories.

1.3. Radiation Dose in Medical Imaging

Radiation safety is a unique and chronically challenging safety issue in radiology that has been mainly exacerbated in the last decades by the increased use of computed tomography (CT).

Ionizing radiation has been used for diagnosis in medicine for more than a century. Diagnostic x-rays are the largest man-made source of radiation exposure

to the general population, contributing about 14% of the total annual exposure worldwide from all sources[9]. The benefits are enormous and clearly exceed the risks. The more recent development of remarkable equipment such as multidetector row CT and the increased utilization of convential radiography and nuclear medicine imaging studies have improved the lives of our patients and, along with other new modalities, revolutionized the practice of medicine.

Over the past quarter century, there has been a rapid growth in both the number of diagnostic x-ray examinations and the introduction of newer, very valuable, but also relatively high-dose technologies [9, 10]. In 1987, medical x-rays and nuclear medicine studies contributed less than 15% of the average yearly radiation exposure received by the US population; the large majority was attributable to radon and other natural sources [9]. Two decades later, because of the dramatic increase in the number of diagnostic examinations performed each year as well as the higher doses associated with these examinations, this fraction has significantly increased. This dramatic evolution of imaging has also resulted in a significant increase in the population's cumulative exposure to ionizing radiation. Whether this will cause an increased incidence of cancer years down the line is currently under debate, the presumption is that it will [9].

Medical radiation from x-rays and nuclear medicine accounts for a mean effective dose (ED) of 3.0 milliSievert (mSv) per person per year, equivalent to the radiation dose of 150 chest X-rays (CXR) [11]. The natural background radiation worldwide is about 2.4 mSv [12]The significant increase in the cumulative exposure of patients and population to ionizing radiation is likely to cause an

increased incidence of cancer in years down the line, with an important yet potentially avoidable public health threat [13]. The balance between risks and benefits determines the appropriateness score of a test; the test is appropriate when benefit greatly exceeds the risks, and inappropriate when risk exceeds the benefit.

Ionizing radiation, especially at high doses, has long been known to increase the risk for developing cancer. In fact, x-rays have recently been officially classified as a "carcinogen" by the World Health Organization's International Agency for Research on Cancer [14]. The most comprehensive epidemiologic study supporting the carcinogenic effect of radiation is that of the atomic bomb survivors in Japan. The data from this study show a statistically significant increase in cancer at dose estimates in excess of 50 mSv [15]. Whether there is a cancer risk at lower doses remains controversial. It is worth noting that many CT scans and nuclear medicine studies have effective dose estimates in the range of 10 to 25 mSv for a single study [16], and some patients have multiple studies; thus, it would not be uncommon for a patient's estimated exposure to exceed 50 mSv. In further validation of this concern, the International Commission on Radiological Protection has reported that CT doses can indeed approach or exceed levels that have been shown to result in an increase in cancer [17].

Although there are currently no data showing that high-dose medical diagnostic studies such as CT and nuclear medicine have actually increased the incidence of cancer, a 2004 study (using survey data from 1991 to 1996) suggested that medical exposure might be responsible for 0.6% of cancers in UK and

approximately 1% of the cancer in the United States [18]. Japan was found to have the highest attributable risks in this study, with 3.2% of the cumulative risk of cancer attributable to diagnostic x-rays, equivalent to 7587 cases of cancer per year [18].This rate can be expected to increase on the basis of the higher number of examinations performed today [9]. On the other hand, as the use of medical radiation has increased, the incidence of some cancers has actually decreased [9].

Cancer induction associated with radiation goes unrecognized because it is neither differentiable nor predictable for individual patients, and because clinically significant consequences do not become evident for many years [13]. Radiation-induced cancers typically do not occur until 1 or 2 decades or longer after exposure [9]. Thus, any increase in cancer occurrence due to burgeoning medical exposures in the past 2 decades, as is the case for CT and nuclear medicine studies, may not be expected to be evident for many years [9]. In addition, because radiation is a relatively weak carcinogen, it is difficult to isolate radiation-induced cancers (1/1,000 per 10-mSv effective dose) that are superimposed on the normal back- ground risk for other cancers (approximately 40% of the population will be diagnosed as having cancer at some point in their lives) [19].

The current annual collective dose estimate from medical exposure in the United States has been calculated as roughly equivalent to the total worldwide collective dose generated by the nuclear catastrophe at Chernobyl [20]Therefore, one can assume, using International Commission on Radiological Protection [17]risk factors, that this annual collective dose may likely result in an increase in the

incidence of imaging-related cancer in the US population in the not-too-distant future. Data analysis shows significant differences in national radiological practices and a very uneven distribution of patient doses amongst the world population. The mean annual effective dose per head of the population varies by up to a factor of 60 between health care level I and IV countries, and still by a factor of approximately 6 within health care level I countries [16].

1.3.1. Radiation dose measurement

When radiation interacts with biological matter, the resulting biological effect depends on the amount of radiation energy absorbed into the material and the type of radiation [21].

1.3.1. 1. Absorbed Dose

Organ dose or organ specific absorbed dose is defined as the energy imparted per unit mass of an organ or tissue [21]. The absorbed dose is measured in grays (Gy), defined as joules per kilogram. The gray replaced the rad (radiation absorbed dose), the traditional unit of absorbed dose, which is equal to 0.01 Gy.

1.3.1. 2. Equivalent dose

Different types of radiation (eg, alpha, beta, neutron, photon) result in different amounts of biological damage, even when the absorbed doses are the same. Some

radiation, including alpha particles, causes a greater amount of damage per unit of absorbed dose than other radiation. The greater the rate at which the radiation transfers energy to tissue, the greater the biological damage [21]. The term equivalent dose was introduced to reflect the different biological effects of different radiation types. The equivalent dose is calculated by multiplying absorbed dose by a "radiation weighting factor." The radiation-weighting factor is unity for the type of radiation (photons) that comes from conventional radiography and computed tomography (CT), and therefore, equivalent dose and absorbed dose are the same for radiation exposure from CT scans. The equivalent dose is measured in sieverts (Sv). The traditional unit of equivalent dose was the roentgen equivalents human (or mam- mal) (rem) (1 rem=0.01 Sv).

1.3.1. 3. Effective Dose

When only a part of the body is exposed (a common situation from medical radiation exposure), the biological damage depends on the exposed organ's sensitivity to that radiation. The International Commission on Radiation Protection (ICRP) introduced the concept of a tissue-weighting factor, which represents the relative contribution of each tissue or organ to the total effects resulting from uniform irradiation of the whole body [21]. Therefore, effective dose is defined as the tissue-weighted sum of the equivalent doses to specified organs and tissues of the body. The effective dose reflects the radiation effects of a nonuniform exposure in terms of an equivalent whole body exposure. It takes into account the absorbed doses received by various organs and tissues and

weighs them according to present knowledge of the sensitivity of each organ to radiation. It also accounts for the type of radiation and the potential for each type to inflict biological damage. The unit of effective dose is the sievert (Sv).

Effective dose can be used to compare radiation exposure across the different types of CT studies and across the different medical study modalities, facilitating comparison of CT to the most common radiology studies patients undergo. It is the most frequently reported measurements to quantify the radiation exposure associated with each CT examination. The effective dose accounts for the amount of radiation to the exposed organs and each organ's sensitivity to developing cancer from radiation exposure.

1.3.2. Estimation of Effective Dose

Effective dose is estimated using the volume computed tomographic dose index (CTDIvol), expressed in milligrays, and the dose-length product (DLP), expressed in milligray- centimeters, which are recorded as part of the CT scan. CTDIvol is a measure of the average dose absorbed by a given phantom at a given scanner output (ie, set of scanning parameters or "protocol"). It is, however, measured from one axial CT scan. Dose-length product, on the other hand, is normalized for the length of the scan and is thus an estimate of the total absorbed dose.

Values of CTDIvol for each protocol are determined by a radiation physicist whenever a new scanner arrives or an existing scanner undergoes major repairs or during periodic quality control assessment [22]. An acrylic phantom is placed at

the isocenter of CT gantry rotation to mimic the scatter properties of human tissues. Different phantoms are used for different applications; for example, the standard body phantom is 32 cm in diameter, whereas a 16-cm phantom is used to mimic either the adult head or the pediatric body, and a 10-cm phantom is used to mimic the pediatric head. Ionization chambers are used to measure radiation exposure in different parts of the phantom, after which a standard formula is applied, ultimately yielding CTDIvol in milligrays [22].

Dose-length product is equal to CTDIvol multiplied by the length of the area scanned in centimeters and is expressed in milligray-centimeters. Dose-length product is especially useful when attempting to convert exposures from the CT dose index (CTDI) to effective dose in sieverts, the universal currency of patient radiation exposure that encompasses the risk for harm from radiation effects models.

The European Working Group for Guidelines on Quality Criteria in CT has proposed a generic estimation method for effective dose [23]. Effective dose is calculated using following formula was used :

$$ED\ (mSv) = DLP\ (mGy \cdot cm) \times k\ [mSv / (mGy \cdot cm)]$$

where DLP is the dose-length product, and *k* is a normalized conversion factor specific for the anatomic region (Table 2). For example, the normalized conversion factors (*k*), for the chest in an adult patient is 0.014 [23, 24]

Table 2. Normalized effective dose per dose-length product (DLP) for adults

(standard physique) and pediatric patients of various ages over various body regions (From Mc Collough [25].

	K (mSv . mGy $^{-1}$. cm $^{-1}$)				
	0 year old	**1 year old**	**5 year old**	**10 year old**	**Adult**
Head and neck	0.013	0.0085	0.0057	0.0042	0.0031
Head	0.011	0.0067	0.0040	0.0032	0.0021
Chest	0.039	0.026	0.018	0.013	0.014
Abdomen and pelvis	0.049	0.030	0.020	0.015	0.015
Trunk	0.044	0.028	0.019	0.014	0.015

It has to be noted that neither CTDI nor DLP represents the dose absorbed by any specific patient; neither is based on any measurement performed while the patient is in the scanner [22]. Instead, both measures provide standardized estimates of average doses to cylindrical phantoms that are useful for comparing average doses between protocols and across imaging centers. These measures are highly precise, but not necessarily accurate when used to estimate the dose to an individual

patient [22]. The uncertainty inherent in translating phantom dose measurements to effective dose for individual patients can be as high as 50% [22]. When these effective doses are further translated to individual cancer risk estimates, further uncertainly is introduced.

An additional caveat involves the importance of the phantom used to make the measurements. Even if all scan parameters are held constant, using different phantoms of different size yields different CTDIvol measurements. Because of soft tissue beam scattering, smaller diameter patients and phantoms will absorb more radiation per unit volume. If a patient is significantly larger or smaller than the phantom used to determine CTDIvol, the measurement will be inaccurate [22]. This issue is most important with regard to pediatric patients who are significantly smaller than the phantoms available at a given institution and who have a higher risk for radiation-induced cancer per exposure unit.

1.4. Biological effects of radiation

Radiation is simply a mechanism whereby energy passes through space. It takes the form of an electromagnetic wave, with the frequency of the electromagnetic wave determining its position in the electromagnetic spectrum [26]. Low-frequency waves such as radio waves lie at one end of the spectrum and high-energy, high-frequency X-rays/Gamma rays at the other end. These high-frequency, high-energy waves are termed “ionizing” (as opposed to non-ionizing) radiation because they contain sufficient energy to displace an electron from its

orbit around a nucleus [26]. The most important consequence of this displaced electron on human tissue is the potential damage it can inflict on DNA, which may occur directly or indirectly [26]. Direct damage occurs when the displaced electron hits and breaks a DNA strand. Indirect damage occurs when the electron reacts with a water molecule, creating a powerful hydroxyl radical which then damages the cell's DNA [26].

Damage to a cell's DNA in either of these ways can have several consequences. A single-strand DNA break is usually repaired appropriately by the cell with no subsequent deleterious sequelae. However, a break affecting both strands of DNA allows the potential for abnormal reconnection of the strands, which likely accounts for all the adverse biological effects ionizing radiation has on humans. First, DNA may rejoin itself incorrectly, rendering the cell nonviable with cell death taking place. Second, it may rejoin as a symmetrical translocation with the potential expression of an oncogene during division (and development of subsequent malignancy) or with abnormal division in gonads, giving rise to potential hereditary disorders [26].

Radiosensitivity is the probability of a cell, tissue, or organ suffering an effect per unit dose of radiation. Radiosensitivity is highest in cells that are highly mitotic or undifferentiated. For this reason the basal epidermis, bone marrow, thymus, gonads, and lens cells are highly radiosensitive. Muscle, bones, and nervous system tissues have a relative low radiosensitivity [26].

There are two main biological effects of radiation: 1) deterministic effects, tissue reactions which happen when the radiation dose exceeds a specific threshold and

become evident days to months after exposure as they cause a predictable change in tissue; 2) and stochastic effects, which relate to the potential for future harm to the tissue and the body [13].

1.4.1. Deterministic effects

Deterministic effects, or tissue reactions, only occur once a threshold of exposure has been exceeded [26]. The severity of deterministic effects increases as the dose of exposure increases. Because of an identifiable threshold level, appropriate radiation protection mechanisms and occupational exposure dose limits can be put in place to reduce the likelihood of these effects occurring.

Early tissue reactions (hours to a few weeks after irradiation) may be of an inflammatory nature, occurring as a result of changes in cell permeability and the release of inflammatory mediators [27]. Subsequent reactions are often a consequence of cell loss (e.g. mucositis and desquamation in epithelial tissues), although non-cytotoxic effects on tissues also contribute to these early reactions. Late tissue reactions (months to years after irradiation) are called ‘generic’ if they occur as a result of injury directly in the target tissue (e.g. vascular occlusions leading to deep tissue necrosis after protracted irradiations), or ‘consequential’ if they occur as a result of severe early reactions (e.g. dermal necrosis as a result of extensive epidermal denudation or chronic infection, and intestinal strictures caused by severe mucosal ulceration) [27]. However, it is important to realize that these two conditions are not mutually exclusive but often coexist.

Tissue reactions of most concern for patients and operators include skin injuries (reported in patients undergoing long, repeated and complicated interventional procedures [13]) and cataract (present in one-third to half of interventional radiologists [13, 28]). The new recommended equivalent dose limit for occupational exposure of the lens of the eye is based on prevention of radiogenic cataracts, with the underlying assumption of a nominal threshold at 0.5 Gy for acute or protracted exposure [27].

1.4.2. Stochastic effects

Current thinking is that stochastic effect occurrence follows a linear no-threshold hypothesis. This means that although there is no threshold level for these effects, the risk of an effect occurring increases linearly as the dose increases [26]. The stochastic effect of most concern is a carcinogenic effect. It occurs when the cell is modified by damage to its DNA but remains viable, the harm eventually being expressed through cell proliferation [29]. Ionizing radiation damages DNA molecule either directly (through ionization of DNA molecule) or indirectly (through generation of free radicals and reactive oxygen species in the surrounding medium). Cancer may occur after a latency period of many years.

The reduction of risk of cancer is at the core of the radiation protection system for patients and staff [13]. The available epidemiological evidence linking increased cancer risk to radiation exposure is now strong for doses >50 mSv [30], also for diagnostic medical exposures. In contemporary imaging practice, doses >50–100

mSv are sometimes reached after cumulative exposures in a single hospital admission and not infrequently by a patient in multiple examinations and diagnostic or interventional procedures for a single imaging technique [31] and even in a single examination [13].

For any given radiation exposure, the cancer risk is higher in females than in males, in children than in adults, and in adults than in elderly, and may differ among individuals [13]. From a radiation sensitivity standpoint, not all tissues have the same risk of radiation-induced cancer.

The radiation-induced cancer is clinically undistinguishable from a spontaneously occurring cancer. Out of 100 subjects exposed to 100 mSv (equivalent to 5000 CXRs), 42 will develop a spontaneous cancer anyway (independently of radiation exposure), and the radiation exposure may induce 1 additional cancer [13]. These estimates have a considerable margin of uncertainty, with a 2 to 3 confidence interval of attributable risk estimates, which translates in the example above into an additional risk as high as 1 in 30 or as low as 1 in 300 [13].

1.5. Computed tomography: doses and risks

CT has become the pre-eminent method of examining patients with ionizing radiation. Because of the versatility provided by newer multidetector CT systems, it is fast replacing the clinical examination of the patient. Integrating CT into routine care has improved patient health care dramatically, and CT is widely considered among the most important advances in medicine. However, CT

delivers much higher radiation doses than do conventional diagnostic x-rays. For example, a chest CT can typically delivers more than 100 times the radiation dose of a routine frontal and lateral chest radiograph [31].

The use of CT for diagnostic evaluation has increased dramatically over the last two decades, from approximately 3 million performed annually in 1980 in the USA to nearly 75 million nowadays for a total population of around 300 million [13]. CT has virtually replaced the IVU, the barium enema, and much diagnostic angiography. In years to come it is possible that low-dose CT may replace even the chest x-ray for a patient with dyspnea.

Radiation exposure from CT examinations has also increased, in part due to the increased speed of image acquisition allowing vascular, cardiac, and multiphase examinations, all associated with higher doses. Thus, greater use of CT has resulted in a concurrent increase in the medical exposure to ionizing radiation [31].

1.5.1 General principles of ALARA

The guiding principles for radiation protection in medicine are: 1) Justification: The exam must be medically indicated; 2) Optimization: The exam must be performed using doses that are As Low As Reasonably Achievable (ALARA), consistent with the diagnostic task; 3) Limitation: While dose levels to occupationally exposed individuals (i.e. the radiologist or technologist) are limited

to levels recommended by consensus organizations, limits are not typical for medically-necessary exams or procedures [32].

As the use of CT is significantly increased, the radiology community has worked to implement the ALARA principles into CT imaging. It has become clear that the responsible use of CT requires the adjustment of several technique factors, mainly based in patient size (attenuation characteristics). The guiding principle for dose management in CT is that the right dose for a CT examination takes into account the specific patient attenuation and the specific diagnostic task. For large patients, this indeed means a dose increase is consistent with ALARA principles. Additionally, each CT exam must be appropriate for the individual patient. Justification is a shared responsibility between requesting clinicians and radiologists [32].

1.5.2 Strategies for CT Dose Reduction

CT scanners create cross-sectional images by measuring x-ray attenuation properties of the body from many different directions. “High-end” CT systems allow acquisition of isotropic volumetric data sets that permit images less than 1 mm thick and high quality reformatted images [32].

In recent years, the dose per examination have showed a clear downward trend, with a reduction of three quarters of radiation dose in the last decade through increasing use of dose-saving measures and evolving scanner technology. Scanner

manufacturers have subsequently implemented several options to appropriately manage or reduce the radiation dose from CT.

1.5.2.1 General strategies

1.5.2.1.1.Tube current modulation

Modulation of the x-ray tube current during scanning is one effective method of managing the dose [25]. Extremely large variations in patient radiation absorption occur with variations in projection angle and anatomic region. Since the projection with the most noise primarily determines the amount of noise on the final image, it is possible to reduce the dose (photons) for other projections without increasing the noise on the final image.

Angular (x- and y-axis) tube current modulation involves variation of the tube current to equalize the photon flux to the detector as the x-ray tube rotates about the patient (eg, from the anteropos- terior direction to the lateral direction) [25].

Longitudinal (z-axis) tube current modulation involves variation of the radiation dose among anatomic regions (eg, shoulders vs abdomen vs pelvis) by varying the tube current along the z- axis of the patient [25]. Unlike angular tube current modulation, in which the tube current is varied cyclically in relation to the starting tube current value, the task of z-axis modulation is to produce relatively uniform noise levels across the various regions of the anatomy. Thus, the operator must select the desired level of image quality for input to the algorithm.

The simultaneous combination of angular and longitudinal (x-, y-, and z-axis) tube current modulation involves variation of the tube current both during gantry rotation and along the z-axis of the patient (ie, from the anteroposterior direction to the lateral direction, and from the shoulders to the abdomen). The operator must still indicate the desired level of image quality by one of the methods described earlier. This is the most comprehensive approach to CT dose reduction because the x-ray dose is adjusted according to the patient-specific attenuation in all three planes [25].

1.5.2.1.2. Automatic exposure control

It is technologically possible for CT systems to adjust the x-ray tube current in real- time in response to variations in x-ray intensity at the detector. The modulation may be fully preprogrammed, occur in near-real time by using a feedback mechanism, or incorporate pre-programming and a feedback loop [32]. These methods of adapting the tube current to patient attenuation, known generically as automatic exposure control (AEC), are analogous to photo-timing in general radiography and have demonstrated reductions in dose of about 20–40% when image quality is appropriately specified. An exception to this trend occurs with obese patients [32]. In large patients, the radiation dose is increased to ensure adequate image quality. However, much of the additional x-ray dose is absorbed by excess adipose tissue [32]. Thus, doses to internal organs do not increase linearly with increases in tube current settings AEC is a broad term that

encompasses not only tube current modulation (to adapt to changes in patient attenuation), but also determining and delivering the "right" dose for any patient (infant to obese) in order to achieve the diagnostic task.

1.5.2.2. Dual energy Computed Tomography

Dual source dual energy CT (DECT) scanners are a recenlty developed generation of CTs which allow the simultaneous acquisition of multidetector CT data with two different photon energy levels. The dual source DECT consists of two x-ray tubes mounted onto the rotating gantry of the scanner with a 90-degree angular offset. Each tube is equipped with a corresponding 64-channel detector. The field of view (FOV) of the B-tube detector array is slightly smaller (26.8cm) compare with the A-tube (50cm) to accommodate it in the limited gantry space. The scanner can be operated in a dual-source or standard single-source multidetector scanning mode.

The use of different energy levels results in different degrees of x-ray attenuation, measured in Hounsfield units (HU), for different materials. The variation in the HU is minimal for soft tissues, but significant for materials with large atomic numbers [33]. DECT thus allows the characterization of iodine, calcium and other materials within tissues by their different absorptiometric characteristics at low and high photon energy levels [33, 34].

On of the main advantages of DECT is the capability to subtract iodine. With this technique, the contribution of iodine to the density of individual voxels is

calculated, and this contributory element can be subtracted from the voxel across the entire data set to result in calculated images termed “virtual non-contrast images” [35]. The virtual non-contrast images reconstructed from contrast-enhanced DE CT acquisition could replace the standard non-enhanced images, and therefore, reduce the radiation dose.

1.6. INTRODUCCIÓN AL PRIMER ARTÍCULO EN EL QUE SE BASA LA PRESENTE TESIS DOCTORAL:

Endoleak detection after endovascular repair of thoracic aortic aneurysm using dual-source dual-energy CT: suitable scanning protocols and potential radiation dose reduction. Flors L, Leiva-Salinas C, Norton PT, Patrie JT, Hagspiel KD. AJR Am J Roentgenol. 2013;200(2):451-60.

Endovascular aortic aneurysm repair (EVAR) has been established as a minimally invasive alternative to open surgical repair for patients with thoracic and abdominal aortic aneurysms. Endoleaks, defined as the persistence of blood flow within the excluded aneurysm sac, are one of the most frequent complications after EVAR. With modern endografts, endoleak prevalence is reported in approximately 4%–11% of EVAR procedures [1-3].

While several imaging techniques have a role in endoleak detection after EVAR, contrast- enhanced CT angiography (CTA) has become the most widely accepted. The optimal CT protocol for endoleak detection has not yet been established, but a multiphasic CTA protocol is generally recommended [4], which usually includes nonenhanced, arterial and delayed phase acquisition. Pre-contrast images are useful in differentiating calcification in the aneurysm sac from endoleak [4,5]. Arterial and delayed phases are usually required because endoleaks have variable flow rates. The delayed phase has proved to demonstrate endoleaks that are not visualized during the arterial phase [5-7]. Although the scan delay most commonly used for the delayed phase ranges from 60 to 120 seconds

after injection of contrast material [8,9], a late delayed (LD) phase of 300 seconds has been recently recommended for optimal detection of low-flow endoleaks [9].

Since endoleaks can develop at any time after EVAR, lifelong imaging surveillance is mandatory. Therefore, with the goal of radiation reduction, the usefulness of the different phases has been widely discussed in the literature [4,6,10]. Eliminating the arterial phase has been proposed because delayed postcontrast imaging has shown to depict endoleak with higher sensitivity than the arterial phase [7].

The recent introduction of dual energy (DE) CT technology may represent an important advantage on this field. Dual source DE scanners allow the simultaneous acquisition of CT data with two different photon energy levels, which results in different degrees of x-ray attenuation, measured in Hounsfield units (HU). DECT allows the characterization of iodine, calcium and other materials within tissues by their different absorptiometric characteristics at low and high photon energy [11,12]. One of the main advantages of DECT is the capability to subtract iodine. With this technique, the contribution of iodine to the density of individual voxels is calculated, and this contributory element can be subtracted from the voxel across the entire data set to result in calculated images termed “virtual noncontrast images” (VNC) [13]. The VNC images could replace the standard nonenhanced images, and therefore, reduce the radiation dose.

Several recent studies have studied the capabilities of DECT angiography for evaluating the aorta [14], aortic aneurysms [15] and follow-up after EVAR[16-19]. It has been shown that the VNC images can be used as a substitute for

precontrast acquisition in the evaluation of endoleaks after endovascular repair of abdominal aortic aneurysms [16,17,19]. A 40-70 second delayed phase was used in these studies. To our knowledge, the capability of DECT in the evaluation of thoracic endovascular aortic repair (TEVAR) for thoracic aortic aneurysm and the use of a DECT LD phase have not been studied previously.

1.7. INTRODUCCIÓN AL SEGUNDO ARTÍCULO EN EL QUE SE BASA LA PRESENTE TESIS DOCTORAL:

Imaging Follow-up of Endovascular Repair of Type B Aortic Dissection with Dual-Source, Dual-Energy CT and Late Delayed-Phase Scans. Flors L, Leiva-Salinas C, Norton PT, Patrie JT, Hagspiel KD. J Vasc Interv Radiol. 2014 Jan 27. pii: S1051-0443(13)01700-4.

The management of Stanford Type B aortic dissection has undergone substantial change over the past decade. Thoracic endovascular aortic repair (TEVAR) is an excellent alternative to conventional surgical intervention, with significantly lower early mortality [1]. One of the primary aims of TEVAR is to achieve false lumen thrombosis and aortic remodeling. Incomplete closure at the primary entry site or distal reentry through intimal tears with subsequent nonclotting of the false lumen portends a poor prognosis [2,3]. Patency of the false lumen may also be related to the presence of endoleaks.

Although not completely established, a multiphasic CT protocol is recommended in the follow-up of TEVAR for type B dissection and it usually includes nonenhanced and arterial phase acquisitions. The first permits to identify high attenuation materials, such as calcifications or hematomas, which may mimic endoleaks on contrast-enhanced images. A delayed phase is able to depict low flow endoleaks that are not visualized during the arterial phase [4-7]. A late-delayed (LD) phase of 300 seconds has demonstrated optimal detection of low-

flow endoleaks [4,8]. We postulate that the LD phase may have additional value in the assessment of the patency of the false lumen.

Lifelong imaging surveillance is required to evaluate the necessity of adjunctive procedures or open surgery in these patients, with the subsequent cumulative radiation dose. Dual-energy (DE) CT technology allows to reduce radiation dose for multiphasic exams. The simultaneous acquisition of CT data with two different photon energy levels permits to subtract iodine and obtain "virtual noncontrast" images [9].These images can replace the precontrast acquisition in the evaluation of endoleaks after endovascular repair of aortic aneurysms [8,10-13].

JUSTIFICACIÓN

El tratamiento endovascular se ha establecido como una alternativa no invasiva a la cirugía abierta en pacientes con aneurismas y disecciones aórticas. Las endofugas, definidas como la persistencia de flujo sanguíneo en el saco aórtico excluido, son una de las complicaciones más frecuentes tras el tratamiento endovascular de aneurismas aórticos, con una prevalencia aproximada del 4 al 11%.

Aunque diferentes técnicas de imagen tienen un papel en la detección de endofugas tras el tratamiento endovascular de aneurismas y disecciones aórticas, la tomografía computarizada (TC) es la más aceptada. El protocolo óptimo de estudio para la detección de endofugas todavía no se ha establecido. Pero generalmente se requiere la adquisición de las imágenes previo a la administración de contraste y una o varias fases tras el contraste intravenoso.

Los pacientes con aneurismas y disecciones de aorta sometidos a tratamiento endovascular requieren controles radiológicos de por vida y, por tanto, una considerable dosis de radiación. La introducción reciente de la TC con doble energía (DE) puede suponer un gran avance al respecto. La adquisición simultánea de las imágenes con dos niveles de energía fotónica distinta permite, entre otras cosas, sustraer el yodo y obtener las denominadas imágenes "virtuales sin contraste" a partir de imágenes adquiridas con contraste. Estas imágenes tienen el potencial de reemplazar a las tradicionales imágenes sin contraste y, por tanto, disminuir la dosis de radiación.

En pacientes con disecciones aórticas tipo B (limitadas a la aorta descendente), el tratamiento endovascular persigue la trombosis completa de la luz falsa y el

consiguiente remodelado aórtico. La falta de trombosis de la luz falsa se correlaciona con un mal pronóstico. El protocolo de estudio en estos pacientes, tampoco está completamente establecido

La trayectoria investigadora del doctorando se ha movido motivada por el principio de la optimización de los exámenes radiológicos; exámenes que deben realizarse usando dosis de radiación tan bajas como sea razonablemente alcanzable (As Low As Reasonably Achievable; principio ALARA). Este principio de seguridad radiológica es especialmente importante en niños, embarazadas y pacientes que van a someterse a estudios radiológicos de por vida, como son los pacientes con aneurismas y disecciones aórticas en seguimiento tras tratamiento endovascular.

La estancia como fellow de investigacion en la Universidad de Virginia (EEUU) dió al doctorando la oportunidad de contar una tecnología de TC inovadora, el TC de doble energia; tecnología que va sufriendo una introducción paulatina en nuestro país.

La justificación de una línea de investigación sobre la utilidad de la TC de doble energía en pacientes con patología aortica tras tratamiento endovascular es la mejora en la seguridad del paciente, persiguiendo conseguir el mejor estudio radiológico que permita detectar todas las potenciales complicaciones mantiendo la menor dosis de radiación posible. Hasta la fecha hay pocos estudios sobre el tema; en concreto, ninguno de ellos ha investigado el papel de la TC de doble energía en pacientes con disecciones o aneurismas de aorta torácica. Así pues la

realización de esta tesis doctoral es pertinente por su aportación a la promoción de la seguridad del paciente.

HIPÓTESIS Y OBJETIVOS

UNIVERSITAS
Miguel
Hernández

3. HIPÓTESIS Y OBJETIVOS

3.1. HIPÓTESIS

En el presente trabajo postulamos la TC de doble energía, mediante su capacidad de obtener "imagines virtuales sin contrate" puede suplantar a la adquisición tradicional sin contraste y, por tanto, disminuir de manera significativa la dosis de radiación a la que se sometenen los pacientes en seguimiento tras tratamiento endovascular de aneurismas y disecciones aórticas. También hipotetizamos que la adquisición de una fase tardía, 300 minutos tras la administración de contraste, es la idónea para la detección de endofugas en estos pacientes. Finalmente postulamos que esta fase tardía puede tener un papel primordial en la valoración óptima de la permeabilidad de la luz falsa, ya que esta puede infraestimarse en la fase arterial.

3.2. OBJETIVOS

3.2.1. OBJETIVO GENERAL

Estudio del protocolo de imagen óptimo con tomografía computarizada de doble energía en el seguimiento de pacientes con aneurimas de aorta torácica y disecciones aórticos sometidos a tratamiento endovascular.

3.2.2. OBJETIVOS ESPECIFICOS

El objetivo de este trabajo de investigación es doble:

-Por un lado, pretende evaluar la capacidad diagnostica del TC-DE, en la detección de endofugas en pacientes con aneurismas de aorta torácica sometidos a tratamiento endovascular. En concreto, investigar si un protocolo bifásico –que incluya una fase arterial y otra tardía (300 segundos)- o un protocolo monofásico –fase tardía– puede reemplazar el protocolo tradicional trifásico y qué reducción de dosis conseguimos con estos protocolos.

-Por otro, investigar el protocolo de imagen óptimo en pacientes con disección aortica tipo B sometidos a tratamiento endovascular, que permita la evaluación tanto de la luz verdadera como de la falsa, y la presencia de endofugas, todo ello con la mínima dosis de radiación. En concreto, pretendemos evaluar la capacidad diagnostica del TC-DE, el valor de una fase tardía para la detección de endofugas y valoración de la luz falsa, y la reducción en la dosis de radiación.

3.2.2.1. OBJETIVOS DEL PRIMER ARTÍCULO EN EL QUE SE BASA ESTA TESIS DOCTORAL:

Endoleak detection after endovascular repair of thoracic aortic aneurysm using dual-source dual-energy CT: suitable scanning protocols and potential

radiation dose reduction. Flors L, Leiva-Salinas C, Norton PT, Patrie JT, Hagspiel KD. AJR Am J Roentgenol. 2013;200(2):451-60.

The purpose of our study was to evaluate the diagnostic performance of dual-source DECT in the detection of endoleaks after TEVAR. Specifically we sought to investigate whether a double phase CT using arterial and LD phases or a single DECT LD phase CT can replace the standard triphasic CT protocol and what extent of radiation dose savings such an approach could provide.

3.2.2.2. OBJETIVOS DEL SEGUNDO ARTÍCULO EN EL QUE SE BASA ESTA TESIS DOCTORAL:

Imaging Follow-up of Endovascular Repair of Type B Aortic Dissection with Dual-Source, Dual-Energy CT and Late Delayed-Phase Scans. Flors L, Leiva-Salinas C, Norton PT, Patrie JT, Hagspiel KD. JVasc Interv Radiol. 2014 Mar;25(3):435-42.

The purpose of our study was to investigate an optimal imaging protocol for the follow-up after TEVAR for type B aortic dissection allowing comprehensive assessment of the true and false lumen and presence of endoleaks with minimal radiation dose. In particular we sought to evaluate the diagnostic performance of DE CT, the value of a LD phase for endoleak detection and false lumen assessment, and reduction of radiation dose

MATERIAL Y MÉTODOS

4. MATERIAL Y MÉTODOS

4.1. MATERIAL Y MÉTODOS DEL PRIMER ARTÍCULO EN EL QUE SE BASA ESTA TESIS DOCTORAL:

Endoleak detection after endovascular repair of thoracic aortic aneurysm using dual-source dual-energy CT: suitable scanning protocols and potential radiation dose reduction. Flors L, Leiva-Salinas C, Norton PT, Patrie JT, Hagspiel KD. AJR Am J Roentgenol. 2013;200(2):451-60.

Patients

All DECT examinations performed at our institution for evaluation after TEVAR between July 2007 and November 2010 were retrospectively reviewed.

The selection of the patients to be performed in the DECT unit was determined by the availability of scanner at the time of the study and by the width of the patient's thorax. If the widest part of the scanned thoracic anatomy exceeded 37 cm on the CT scout, the patient was disqualified due to internal FOV limits of the CT unit. Additional exclusion criteria were the institutional standard for contrast-enhanced CT: calculated glomerular filtration rate <45mL/min and known adverse reaction to iodinated contrast material.

This study was approved by the local institutional review board with waiver of consent and was compliant with HIPAA regulations.

CT Acquisition

All the examinations were performed using a dual source DECT (Somatom Definition, Siemens Medical Systems, Forchheim, Germany). The dual source DECT scanner consists of two x-ray tubes mounted onto the rotating gantry with a 90-degree angular offset. Each tube is equipped with a corresponding 64-channel detector. The field of view (FOV) of the B-tube detector array is smaller (26.8cm) than that of the A-tube (50cm) due to limited gantry space. The scanner can be operated in DE or standard single-source multidetector scanning mode.

Our standard triple-phase CT protocol was performed in all cases. This consisted of an unenhanced acquisition, an arterial phase, and a LD phase, all of them acquired in inspiratory breath-hold.

The initial unenhanced acquisition was acquired with a single-source configuration (collimation, 24x1.2mm; tube current-time product, 225 mAs; tube potential 120 kVp; rotation time, 0.5 sec; pitch, 0.9). The area of coverage in this acquisition ranged from 3cm above the stent to 1cm below it.

An arterial phase was acquired with a single-source configuration (collimation, 64x0.6mm; tube current-time product, 300 mAs; tube voltage 120 kVp; rotation time, 0.5 sec; pitch, 0.9) after the intravenous injection of 100 mL of non-ionic iodinated contrast agent (Omnipaque 350; GE Healthcare, Princeton, NJ, USA) at a rate of 4 cc/sec followed by a chaser bolus of 25mL of saline solution. The scan delay was determined using a bolus-tracking technique (CareBolus software; Siemens Medical Solutions) by placing a region of interest (ROI) in the ascending aorta and simultaneously starting the dynamic monitoring

scan and the intravenous contrast material injection. The trigger threshold inside the ROI was set at +125 HU (Hounsfield Units) absolute value. The arterial phase acquisition range was usually from the pulmonary apex to the lowest point of the diaphragm. Depending on the clinical justification, part of the abdomen was also covered in some cases.

A DE LD phase scan was acquired 300 seconds after the beginning of the contrast material injection. The CT mode was Spiral DE with Dual Source. Tube voltage for tube A was set to 140kVp with a tube current-time product of 100mAs, and the tube voltage for tube B was 80kVp with a tube current-time product of 425mAs. The collimation was 14x1.2 mm; gantry rotation time was 0.5 s, and pitch 0.7. Similar area of coverage as in the unenhanced acquisition was used. In order to make the DECT scan protocol radiation neutral compared to our standard single-energy protocol, the CTDI of the DE acquisition was tailored to match the CTDI of our routine single-energy delayed acquisition. We acquired the venous phase at 300 seconds (LD phase), instead of the frequently used 60 seconds (early delayed phase), because this timing has been shown to be the optimal for low-flow endoleak detection [9]. We acquired the delayed rather than the arterial phase with DE according with previous data that has shown that this modality is accurate for the detection of endoleaks missed during the arterial phase [7].

Attenuation–based dose modulation (CareDose4D; Siemens) was used in all cases to ensure delivery of lowest radiation dose and production of diagnostic scans.

CT Data Postprocessing

Unenhanced images and arterial images were reconstructed and available for review with a slice thickness of 5mm and a section of increment of 5mm, and 1mm of thickness and 1mm of increment respectively.

From the raw spiral projection data of both tubes in the DE LD acquisition, three separate datasets were generated: images at 80kVp, 140kVp, and weighted average (WA) images (consisting of 30% of 80kVp and 70% of 140kVp information, which resulted in images with characteristics comparable to a 120kVp image data set). Of each of these datasets, two series of images were then reconstructed with a slice thickness of 0.6mm and 5mm, and a section of increment of 0.6mm and 5mm respectively. The images with a slice thickness of 5mm and a section of increment of 5mm were selected for primary review; the 0.6mm images were only used when deemed necessary by the reviewer.

A soft-tissue convolution kernel B30f was applied to the unenhanced and arterial phase image, and a D30f for DE LD phase images.

DE data were post-processed on a workstation (Multimodality Workplace, Siemens Medical Systems, Forchheim, Germany) running Syngo software version VA 11. For the generation of DECT-based VNC images, a DE postprocessing preset called “Liver VNC” was used. This application is based on the 3-material decomposition algorithm. VNC CT data, an iodine data set, and a color-coded data set that shows iodine distribution overlay the VNC image or WA image were obtained.

Data Interpretation: Reading sessions

The cases were retrospectively evaluated by two independent radiologists (K.D.H. and L.F., with 22 and 6 years of experience in body CT) who were blinded to the patient's clinical information and previous imaging findings. Axial images as well as multiplanar reconstructions were reviewed on external workstations.

Three different reading sessions were performed. In all reading sessions the data sets were anonymized and analyzed in random order.

In the first session (session A) the following information of the triphasic protocol was used: true noncontrast, arterial phase, and DE delayed LD phase WA image datasets. This information was considered the reference standard for the diagnosis of endoleak as it is similar to our routine clinical protocol. The interval between reading session A and B was 3 weeks.

In the second session (session B), the readers used VNC instead of the true nonenhanced exam and the DE delayed phase datasets (80kVp, 140kVp and WA images). Immediately after reviewing and recording the final diagnosis for each case in reading session B, the readers reviewed the arterial phase images and recorded the results for the combination of VNC, arterial phase and all three DE delayed phase datasets as reading session C.

For each individual case, the presence of an endoleak was assessed. An endoleak was defined as the presence of contrast material within the aneurysm sac beyond the graft on the arterial or delayed phase, and absence of contrast in the corresponding location on the unenhanced image, virtual or standard. Endoleaks were classified as previously described [20-22]: type I, leak due to incomplete

attachment of the proximal or distal portion of the prosthesis caused by technical or anatomic problems; type II, leak due to retrograde flow into the aneurysm sac via aortic collateral arteries; type III, leak due to graft defect or a graft module disconnection; and Type IV, leak due to porosity of the prosthesis.

Both readers scored their level of confidence in endoleak detection as: 1, low confidence; 2, high confidence.

The readers assessed the endoleak size. For this purpose, a visual quantification of the endoleak was made as an estimate percentage area of the aneurysm sac using a four-point scale [23]: 1, <3% of the aneurysm sac; 2, >3% but <10%; 3, >10% but <30%; and 4, >30%.

In cases of disagreement between the two readers the final decision was performed by consensus.

Endoleaks detected only on LD phase CT were classified as low-flow leaks [9,24]. When arterial and venous phases were analyzed together, the phase in which the endoleak was qualitatively better seen was recorded. The detectability of endoleaks in each LD DECT dataset was also qualitavely analyzed by recording the dataset that provided better depiction.

Direct Comparison Virtual Non-Contrast and Standard Nonenhanced

Erroneous subtraction of calcification within the aneurysm sac on VNC images can mimic an endoleak. Therefore, in order to evaluate the ability of three-material decomposition to correctly remove iodine from DE images without significant calcification subtraction, one of the radiologists (L.F) assessed the level of calcium subtraction on VNC in comparison to the true unenhanced

acquisition using a previously described [19] five-point scale: 1, no subtraction; 2, minimal subtraction of focal calcifications; 3, moderate subtraction of focal calcifications; 4, severe subtraction of large calcifications; and 5, subtraction of all calcifications.

Tissue attenuation and Contrast-to-Noise Ratios

The attenuation in the lumen of the thoracic aorta at the level of the endograft and the attenuation of the thrombus in the adjacent aneurysm sac were measured by drawing circular regions of interest (ROIs) in the same z axis position. The diameter of the ROI was made as large as possible depending on the anatomic region. ROIs of similar size were placed at the same location on standard nonenhanced, arterial phase, venous phase (80kVp, 140kVp and WA) and VNC images. The average attenuation was recorded for all datasets.

If an endoleak was present, ROI measurements within the leak were also performed for the arterial phase and the three delayed phase datasets. The attenuation in the adjacent aneurysm sac was also recorded.

Since surrounding air was absent for attenuation measurements in most of the 80kVp images due to the smaller FOV of the B tube, image noise was calculated as the SD of an ROI placed in an area of homogenous subcutaneous fat in the same z axis position as the attenuation measurements in all the datasets.

These measurements were obtained in one session by a single radiologist (C.L.S.)

The contrast-to-noise ratios (CNRs) in the aorta were calculated for the arterial and the three LD datasets using the following equation [17]:

$$CNR = (A_A - A_S) / N,$$

where A_A and A_S are the mean attenuation of the aortic lumen and the adjacent aneurysm sac respectively, and N is the noise. In addition, the CNRs in the endoleaks were similarly calculated by using the formula:

$$CNR = (A_L - A_S) / N,$$

where A_L is the mean attenuation of the leak.

Radiation dose Measurements

For each of the CT acquisitions, individual effective doses (ED) were calculated from the dose-length products (DLP), which were recorded from the patient protocol. Normalized conversion factors (*k*), 0.014 for the chest, were used to calculate the ED [25], and the following formula was used:

$$ED\ (mSv) = DLP\ (mGy \cdot cm) \times k\ [mSv / (mGy \cdot cm)]$$

For this analysis, in order to simplify and to be able to work with a single organ-specific conversion factor, we excluded patients whose SECT included part of the abdomen.

Statistical Analysis

Inter-session diagnostic agreement analyses were conducted to investigate whether a double-phase acquisition using arterial and DE LD phases or a single DECT LD phase acquisition can replace the standard triple-phase protocol. The diagnostic agreement analyses were carried out in the traditional 2 x 2 cross-classification table framework and were based on inter-rater classification consensus. The consensus classifications from the standard triphasic CT protocol served as the gold standard classifications in the agreement analysis.

For each *inter-session* diagnostic agreement analysis, the following summary measures of diagnostic agreement were estimated based on the 2 x 2 cross-classification table cell frequencies: 1) absolute inter-session diagnostic agreement (%), and 2) sensitivity, 3) specificity, 4) positive predicted value, and 5) negative predicted value of the of the non-gold standard diagnostic method. Confidence interval construction for each summary measure was carried out using the Clopper and Pearson exact method [26]**,** and when at least one of the two off-diagonal cell frequencies of the 2 x 2 frequency table was non 0, the McNemar exact-test was utilized to test for non-randomness, with respect to diagnostic discordance (note that when both off-diagonal cell frequencies of the 2 x 2 table are equal to 0, the McNemar statistic is undefined).

For each reading session, *inter-observer diagnostic agreement* was assessed by way of the conventional Kappa statistic (*k*), and the McNemar exact-test. The Clopper and Pearson exact method was utilized to estimate the lower and the upper 95% confidence limits for the absolute inter-rater diagnosis agreement (%).

The aorta CNR data and the endoleak CNR data were analyzed separately via linear-mixed effects models. In each analysis, the means of the distributions of the CNRs measurements were compared between the arterial, 80 kVp, 140 kVp, and WA delayed phase data in a pairwise manner. Pairwise testing of the mean CNR under the different delayed phase datasets was based on the Tukey's multiple comparison type I error rate decision rule [27], in which the two-sided experiment wise type I error rate was set *apriori* at 0.05.

The *inter-session* diagnostic agreement analyses and the *inter-rater* agreement analyses were conducted via the FREQ procedure of SAS version 9.2 (SAS Institute Inc., Cary, NC). CNR data analyses were conducted via the MIXED procedure of SAS version 9.2.

4.2. MATERIAL Y MÉTODOS DEL SEGUNDO ARTÍCULO EN EL QUE SE BASA ESTA TESIS DOCTORAL:

Imaging Follow-up of Endovascular Repair of Type B Aortic Dissection with Dual-Source, Dual-Energy CT and Late Delayed-Phase Scans. Flors L, Leiva-Salinas C, Norton PT, Patrie JT, Hagspiel KD. Vasc Interv Radiol. 2014 Mar;25(3):435-42.

Patients

We retrospectively reviewed all DE-CT studies performed consecutively at our institution for follow-up after TEVAR of type B dissections in a 42-month period. Availability of the DE CT scanner at the time of the study determined the selection of the patients to be performed in this unit. Due to the internal field of view (FOV) restrictions of the scanner, the thoracic width of the patient was also a determinant factor. If it exceeded 37 cm on the CT scout image, the patient was excluded. A glomerular filtration rate under 45mL/min and a known allergy to iodinated contrast material were also exclusion criteria. Our institutional review board approved the study with waiver of consent and it was compliant with HIPAA.

CT Acquisition

All CT studies were acquired with a dual-source DECT scanner (Somatom Definition, Siemens Medical Systems, Forchheim, Germany) which consists of two x-ray tubes with corresponding 64-channel detector with an angular offset of

90°. The B-tube detector array has a smaller field of view (FOV) than the A-tube (26.8cm vs. 50cm). Both tubes can be operated independently, allowing to operate the scanner in standard single-source or dual-source mode. Attenuation–based dose modulation (CareDose4D; Siemens) was used in all cases.

Our standard triple-phase protocol (unenhanced acquisition, arterial phase, and late delayed phase) was performed in all cases. The unenhanced acquisition was acquired with a single-source configuration (collimation, 24x1.2mm; tube current-time product, 225 mAs; tube potential 120 kVp; rotation time, 0.5 sec; pitch, 0.9) and an area of coverage limited to the stent graft (from 3cm above the stent to 1cm below it).

The arterial phase was also acquired with a single-source configuration (collimation, 64x0.6mm; tube current-time product, 300 mAs; tube voltage 120 kVp; rotation time, 0.5 sec; pitch, 0.9) following the intravenous administration of 100 mL of non-ionic iodinated contrast agent (Omnipaque 350; GE Healthcare, Princeton, NJ, USA) with an infusion rate of 4 cc/sec using bolus tracking at the level of the ascending aorta (CareBolus software; Siemens Medical Solutions). The arterial phase covered from the pulmonary apex to the lowest point of the diaphragm or the iliac crests, depending extent of the dissection.

A DE LD phase scan was acquired with a 300 second delay after the contrast material administration. The CT mode was Spiral Dual-Energy with Dual-Source, tube voltages were set at 140 kVp (tube A) and 80 kVp (tube B) and the current-time products were 100mAs (tube A) and 425mAs (tube B). Collimation was 14x1.2 mm; gantry rotation time was 0.5 s with a pitch of 0.7.

The area of coverage of this phase was similar to the unenhanced acquisition. To ensure similar radiation exposure with the DECT protocol compared to our single-energy clinical protocol, we adapted the CTDI of the DE acquisition to match with the CTDI of our routine single-energy delayed acquisition. We chose a 300 second delay because it proved to be the optimal for low-flow endoleak detection [4].

CT Data Postprocessing

Three different datasets were generated from the raw spiral projection data of both tubes in DE LD acquisition: 80 kVp, 140 kVp, and weighted-average (WA) images (30% from 80 kVp data and 70% from140 kVp data; rendering images comparable to 120-kVp). DE data were post-processed on a workstation (Multimodality Workplace, Siemens Medical Systems, Forchheim, Germany) by using dedicated DE software (Syngo, version VA 11). Virtual noncontrast images were obtained with the "Liver VNC" postprocessing preset.

Data Interpretation

Two independent radiologists (with 22 and 6 years of experience in body CT), blinded to the patient's clinical information and previous imaging studies, retrospectively reviewed the cases on three reading sessions. The datasets were anonymized and analyzed in random order.

The first session (session A) was considered the reference standard because it used our routine clinical triphasic protocol: true noncontrast, arterial, and DE delayed phase WA image datasets. There was a 3-weeks interval between reading session A and B.

In the second session (session B), the readers used virtual noncontrast, instead of standard unenhanced, and the arterial phase. We consider this session a single-phase protocol but it has to be noted that the virtual noncontrast images were not truly derived from the arterial but from the delayed phase. We acquired the delayed phase with Dual-Source because the protocol was already set for an ongoing project at our institution looking to replace the triphasic protocol with a delayed phase single-phase protocol in the assessment of endoleaks after endovascular repair of aortic aneurysm. Such an approach would not be valid in the follow-up after endovascular repair of aortic dissection because the arterial phase is mandatory for assessment of the adequate flow in true lumen and its major branch vessels as visceral ischemia is a potential complication.

Immediately following reading and recording the data for a patient in session B, the readers reviewed the delayed phase datasets and recorded the results for the combination of virtual noncontrast, arterial phase and DE late delayed phase datasets (80 kVp, 140kVp and WA image). This was considered reading session C (dual-phase protocol).

The reviewers assessed the presence of endoleak defined as the presence of contrast material beyond the graft within the false lumen on the arterial or venous phase, and its absence in the corresponding location on the unenhanced image, standard or virtual. As previously described [10], endoleaks were classified: type I, leak due to inadequate seal at the graft proximal (A) or distal (B) ends; type II, leak due to retrograde flow via collateral arteries; type III, leak due to a mechanical failure of the graft; and Type IV, leak due to porosity of the graft.

Endoleaks depicted only in the delayed phase were classified as low-flow endoleaks [4].

The readers visually assessed the patency of the false lumen by using a five-point scale: 1, complete patency (complete contrast opacification of the false lumen); 2, partial patency >50% (presence of contrast within more than 50% of the overall false lumen volume); 3, partial patency <50% (presence of contrast within less than 50% of the false); 4, complete thrombosis (absence of contrast within the false lumen); and 5, false lumen collapse (complete remodeling of the false lumen). In cases of disagreement between the two readers in endoleak detection or patency of the false lumen, the final decision was achieved by consensus.

Radiation dose Measurements

Effective dose (ED) was calculated for each CT acquisition using the following formula [14]:

$$ED\ (mSv) = DLP\ (mGy \cdot cm) \times k\ [mSv / (mGy \cdot cm)]$$

where DLP is the dose-length product,and *k* the normalized conversion factor. For the unenhanced and delayed phase acquisition, a *k* specific for the chest of 0.014 was used [15]. Since a combination of thoracic [*k* chest=0.014mSv / (mGy · cm)] and abdominal [*k* abd=0.015mSv / (mGy · cm)] acquisitions was performed in the arterial phase, the mean of both region-specific conversion factors [*k* =0.0145mSv/ (mGy · cm)] was used, as previously described [10].

Statistical Analysis

Inter-session diagnostic agreement analyses were conducted to investigate whether a double-phase or a single-phase protocol can replace the standard triple-phase protocol. The diagnostic agreement analyses were carried out in the traditional 2 x 2 cross-classification table framework and were based on inter-rater classification consensus. The consensus diagnosis from the triphasic protocol served as the gold standard.

For each *inter-session* diagnostic agreement analysis it was estimated:1) absolute diagnostic agreement (%), 2) sensitivity, 3) specificity, 4) positive predicted value (PPV), and 5) negative predicted value (NPV). Confidence intervals were obtained using the Copper and Pearson exact method (16), and when at least one of the two off-diagonal cell frequencies of the 2 x 2 frequency table was non 0, the McNemar exact-test was used to test for non-randomness, with respect to diagnostic discordance. Note that when both off-diagonal cell frequencies of the 2 x 2 table are equal to 0, the McNemar statistic is undefined. For each session, *inter-observer diagnostic agreement* was assessed by conventional Kappa statistic (*k*), and McNemar exact-test. The Copper and Pearson exact method was utilized to estimate the lower and the upper 95%-confidence limits for the absolute inter-observer diagnosis agreement (%). The *inter-session* and *inter-observer* agreement analyses were conducted via the FREQ procedure of SAS version 9.2 (SAS Institute Inc., Cary, NC).

For the assessment of the patency of the false lumen, the agreement between the scores of session B and C and the scores of session A was determined by cross tabulation. The Copper and Pearson exact method was utilized to

estimate the lower and the upper 95%-confidence limits for patency score agreement (%).

RESULTADOS

5.RESULTADOS

5.1. RESULTADOS DEL PRIMER ARTÍCULO EN QUE SE BASA ESTA TESIS DOCTORAL:

Endoleak detection after endovascular repair of thoracic aortic aneurysm using dual-source dual-energy CT: suitable scanning protocols and potential radiation dose reduction. Flors L, Leiva-Salinas C, Norton PT, Patrie JT, Hagspiel KD. AJR Am J Roentgenol. 2013;200(2):451-60.

During the 30-month study period, 48 patients (28 men, 20 women; mean age, 66 years; age range, 19-84) who previously had undergone endovascular repair of thoracic aortic aneuryms (n=41) or pseudoaneurysms (n=7) underwent 74 triple-phase CT examinations. In 15 of these examinations (20%) part of the abdomen was imaged. One case was excluded due to suboptimal opacification of the aorta. Average time interval between EVAR and CT examination was 524 days (range, 3-1638 days).

Reading Session A

Session A, considered the reference standard, revealed endoleaks in 21 of the 74 studies (28.4%). The endoleaks were detected in 14 of the 48 patients (29.1%) and were classified as type II in all the cases. Type I, III and IV endoleaks were not detected. Interobserver agreement for endoleak detection in this session was excellent (k =0.86; 95% CI: [0.73, 0.99]), with an absolute

agreement of 94.6% (95% CI: [86.7, 98.5%]). A consensus reading was required for 4 patients. The level of confidence for the detection of endoleak was high in 70 cases (94.6%). The endoleaks were quantified as: <3% in 5 cases (23.8%), 3-10% in 9 cases (42.9%), 10-30% in 6 cases (28.6%), and >30% in 1 case (4.8%). Four endoleaks were classified as low-flow endoleaks (19%) (Fig.1). 7 endoleaks (33.3%) were better seen on the arterial phase, and 5(23.8%). on the delayed phase.

Fig 1.— Low-flow Endoleak. 79-year old male with low-flow type II endoleak arising from a bronchial artery in a follow-up CT 326 days after TEVAR. Standard nonenhanced (a), arterial phase (b) and DE WA delayed phase (c). Presence of contrast within the aneurysm sac beyond the graft (arrows) is correctly depicted on a 300 seconds delayed phase axial image (c) representing a slow flow endoleak not present on the arterial phase (b).

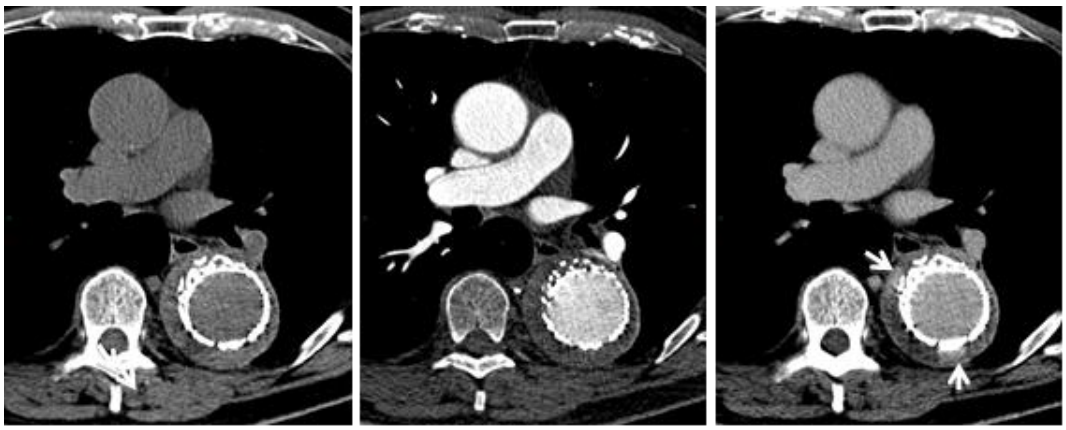

Reading Session B

Using data from only the DE delayed phase acquisition (VNC, and DE LD phase) 18 of the 21 endoleaks (85.7%) were correctly depicted.

The endoleaks were detected in 12 of the 48 patients (25%) and were classified as type II in all the cases. Inter-observer agreement for endoleak detection in this session was high (*k*=0.78; 95% CI: [0.62, 0.94]), with an absolute agreement of 91.9% (95% CI: [83.2, 97.0%]). A consensus reading was required for 6 patients. The level of confidence for the detection of endoleak was high in 64 cases (86.5%). All endoleaks were qualitatively equally well depicted on the 80kVp and WA delayed phases.

There were no false-positive (FP) findings. Three patients had false-negative (FN) image interpretations. All of them were type II endoleaks <3% (Fig.2). Artifact from embolization material was present in one of the FN cases (Fig.3). Decrease in the size of the thoracic aneurysm sac and absence of complications were found in all 3 FN cases on 12-month follow-up CT. None of the FN cases were attributed to incorrect iodine removal on the VNC images.

Fig 2.— Reading Session B False Negative Case. 81-year old female with small type II endoleak on a follow-up CT 357 days after TEVAR. Standard nonenhanced (a), VNC (b), arterial phase (c), 80kVp (d) and WA (e) DE delayed phase images are shown. Presence of contrast material within the aneurysm sac beyond the graft (arrow) is shown on the arterial (c) and delayed phase (d, e) axial images. Absence of high attenuation material in the corresponding location is correctly depicted on the standard (a) and virtual (b) unenhanced images. The

endoleak CNR was 172.7 for the arterial phase, 109.7 for the 80kVp delayed phase, and 88.2 for the WA 120-equivalent delayed phase. Although the endoleak was retrospectively evident on the delayed phase imaging, its lower CNR on this phase when compared to the arterial phase may explain the fact that it was missed.

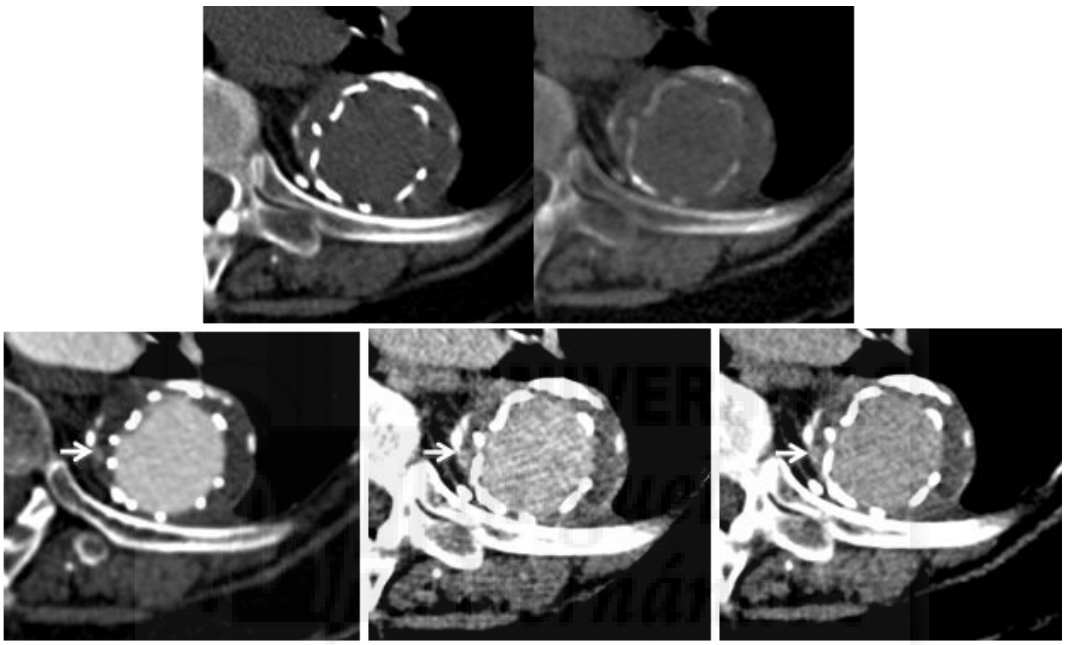

Fig 3.— Reading Session B False Negative Case. 61-year old male with small type II endoleak. Follow-up CT 230 days after TEVAR . Standard nonenhanced (a), VNC (b), arterial phase (c), and DE WA delayed phase (d) images are shown. Presence of contrast material within the aneurysm sac beyond the graft (arrow) is present on both arterial (b) and delayed phase (d), but more conspicuous on the arterial images. There is absence of high attenuation material in the corresponding location both on the standard (a) and virtual (b) unenhanced images. Note the large beam hardening artifact related to embolization material from previously

treated endoleak, which, in addition to the lower endoleak CNR on the delayed phase, may contribute to the false negative finding.

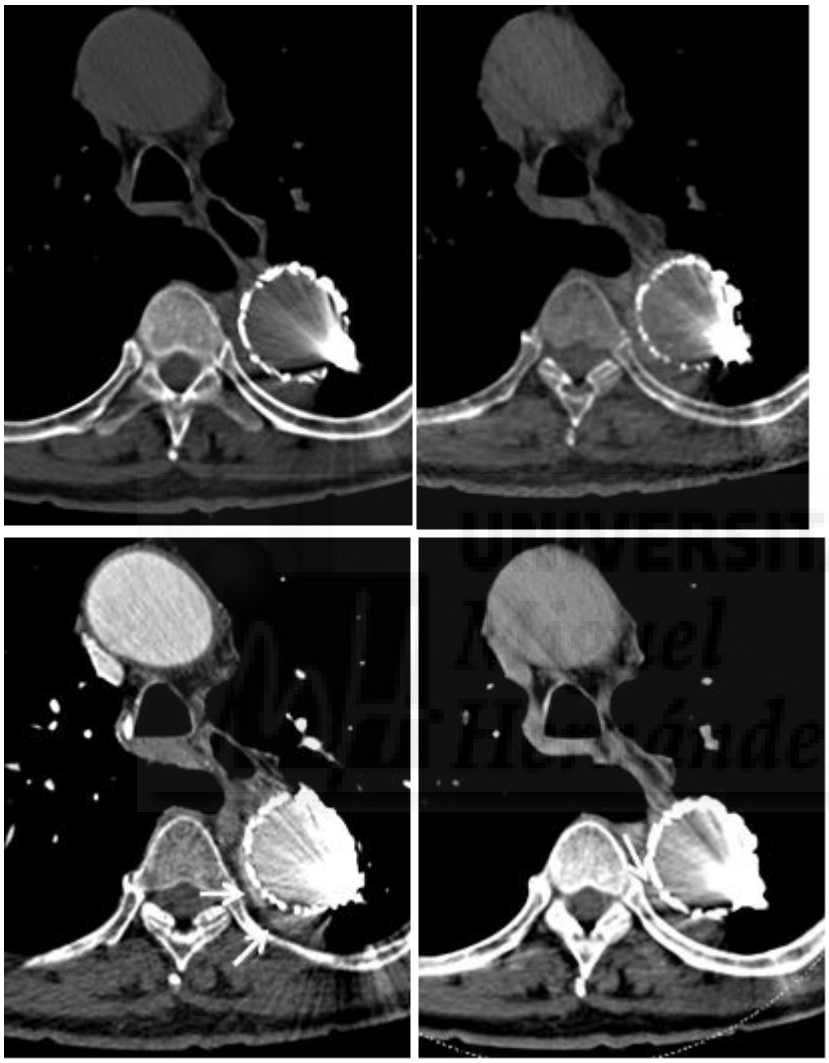

The diagnostic accuracy of reading session B, as compared with the reference standard (session A) is shown in table 1. Agreement between reading session A and B regarding the presence or absence of endoleak was excellent (*k*=0.90; 95% CI: [0.78, 1.00). No significant differences in endoleak detection accuracy between sessions B and A were found (p=0.25). No significant

differences in the level of confidence between sessions B and A were found (p=0.11).

Table 1. Diagnostic Performance of Reading Session B and C as Compared to the Reference Standard (Session A)

Reading Session	Absolute agreement	Sensitivity	Specificity	NPV	PPV
B	95.9% (95% CI: [86.7, 98.5%])	85.7% (95% CI: [63.6, 96.9%]),	100% (95% CI: [93.2, 100%]),	100% (95% CI: [81.5, 100%]),	94.6% (95% CI: [85.1, 98.9%])
C	100% (95% CI: [95.1, 100%])	100% (95% CI: [83.9, 100%])	100% (95% CI: [93.3, 100%])	100% (95% CI: [81.5, 100%])	100% (95% CI: [83.9, 100%])

NPV= Negative Predictive Value
PPV= Positive Predictive Value

Reading Session C

Session C (VNC, arterial phase and DE LD phase) correctly depicted all 21 endoleaks (100%). The endoleaks were detected in 14 of the 48 patients (29.1%) and were classified as type II in all the cases. Inter-observer agreement for endoleak detection in this session was high (*k*=0.71; 95% CI: 0.78 [0.54, 0.84]), with an absolute agreement of 87.8% (95% CI: [78.1, 94.3%]). A consensus reading was required for 8 patients. The level of confidence for the detection of endoleak was high in 70 cases (94.6%). There were no FP or FN findings.

The diagnostic accuracy of reading session C, as compared with the reference standard is shown in table 1. There was perfect agreement between reading session C and A regarding the presence or absence of endoleak, hence no significant differences in endoleak detection accuracy between session C and A were found. No significant differences in the level of confidence between session C and A were found (p=1.00).

Agreement between reading sessions B and C regarding the presence or absence of endoleak was excellent (*k*=0.90; 95% CI: [0.78, 1.00]), with an absolute agreement of 95.9% (95%CI: [88.6, 99.1%]. No significant differences in endoleak detection accuracy between session B and C were found (p=0.25).

Visual Comparison of VNC and Standard Nonenhanced

Within the 74 standard unenhanced datasets, ten did not show aortic calcifications (13.5%). Within the remaining 64 studies, the level of calcium subtraction on VNC images when compared to the standard nonenhanced images was rated as: no calcium subtraction in 29 cases (45.3%), minimal calcium subtraction in 29 (45.3%), moderate in 5 (7.8%) and severe in 1 case (1.6%) (Fig.4). On average, the level of calcium subtraction was rated as 1.65 ± 0.69 (none-minimal).

Fig 4.— Calcification subtraction on VNC image. Comparison of true standard unenhanced (a) and virtual noncontrast (b) image in a 74-year-old female with post-traumatic pseudoaneurysm undergoing a follow-up CT 230 days after

TEVAR. The stent-graft and subtle calcifications of the aortic wall appear less dense on VNC. One focal linear calcification is completely subtracted (arrow), and was rated as moderate calcium subtraction.

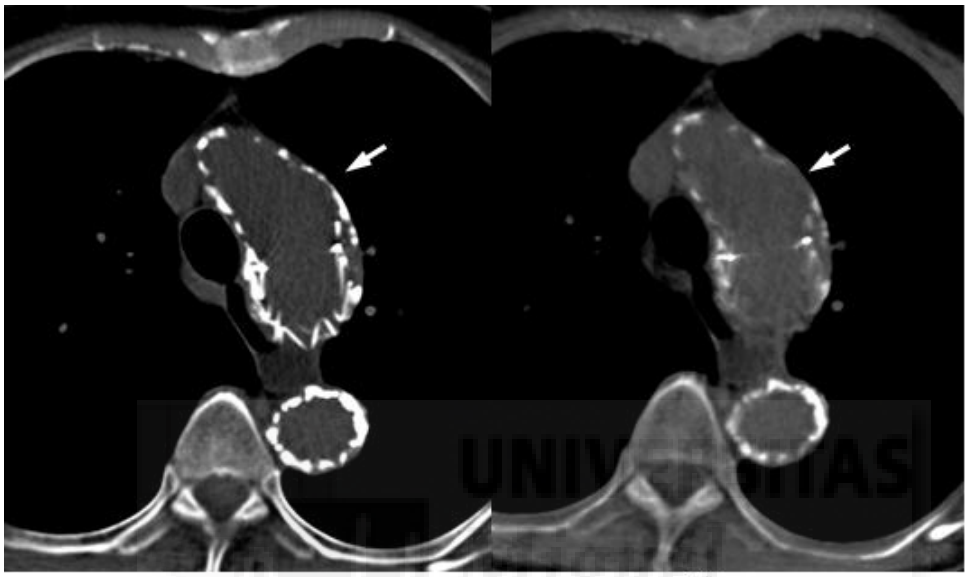

Due to the limited FOV of the B tube, the aneurysm sac was partially outside the FOV in 2 cases (2.6%).

Tissue attenuation and Contrast-to-Noise Ratios

Luminal aortic attenuation on VNC images (45.54 ±17.58 HU, mean ± SD) showed no significant difference when compared with that on true unenhanced images (45.64 ±19.29 HU) (p=0.97).

Thrombus was present and measured outside the stent in 46 of the 74 studies; therefore 28 cases were excluded from the CNR calculations, in 2 of these an endoleak was present. Measurements of attenuation, noise and CNR are given in table 2.

Table 2. Vascular Attenuation, Image Noise and Contrast-to-Noise Ratio at Different Phases and Photon Energy Levels

	Aortic Lumen Attenuation (HU) (n=74)	**Endoleak Attenuation (HU) (n=19)**	**Aneurysm sac Attenuation (HU) (n=47)**	**Noise (SD subcutaneous fat) (n=74)**	**CNR Aorta (n=47)**	**CNR endoleak (n=18)**
120-kVp arterial phase	**335.47 ± 71.16**	**200.75 ± 84.43***	**36.79 ± 16.28**	**19.53± 5.86**	**16.33 ± 5.94**	**9.53±.5.86**
80-kVp delayed phase	**162.56 ± 40.26**	**135.99 ± 30.79**	**42.04 ± 16.67**	**16.93 ± 7.70**	**8.23 ± 4.17**	**6.24 ± 3.46**
140-Kvp delayed phase	**96.67 ± 20.56**	**82.93 ± 19.8**	**36.33 ± 17.55**	**13.97± 6.82**	**4.84 ± 1.96**	**3.62 ± 2.22**
Weighted-average delayed phase	**114.16 ± 31.99**	**98.46 ± 21.38**	**37.97 ± 15.8**	**11.65 ± 3.41**	**7.41 ± 3.72**	**5.68 ± 3.21**
Data are mean values ± standard deviations **CNR= Contrast to Noise ratio** *** Only 15 of the 18 endoleaks were detected during the arterial phase**						

The aortic lumen CNR was significantly higher during the arterial phase when compared to the three delayed datasets ($p<0.001$ for all comparisons). For the delayed phase datasets, aortic lumen CNR in 80kVp images was not significantly different from the WA ($p=0.75$) (Fig.5).

Fig 5.— Aortic CNR comparison between different phases and photon energy levels. A) Box and whisker plot of the distributions of the aorta CNR measurements under the different phase and photon energy levels. B) 95% confidence intervals for the mean differences in aorta CNR between the different phases and photon energy levels. Note that the confidence interval furthest to the left is for the difference between the mean arterial phase CNR and mean 80 kVp

delayed CNR (i.e. mean Arterial CNR - mean 80 kVp delayed CNR) and the confidence interval furthest to the right is for the difference between the mean l40 kVp delayed phase CNR and the mean WA delayed CNR. Also note that the dotted vertical segment of the confidence interval denotes the 95% confidence interval when the length of the interval is not adjusted for multiple comparisons, while the combined length of the dotted and solid vertical segment of the confidence interval denotes the 95% confidence interval when the length of the interval is adjusted for a total of 6 paired comparisons.

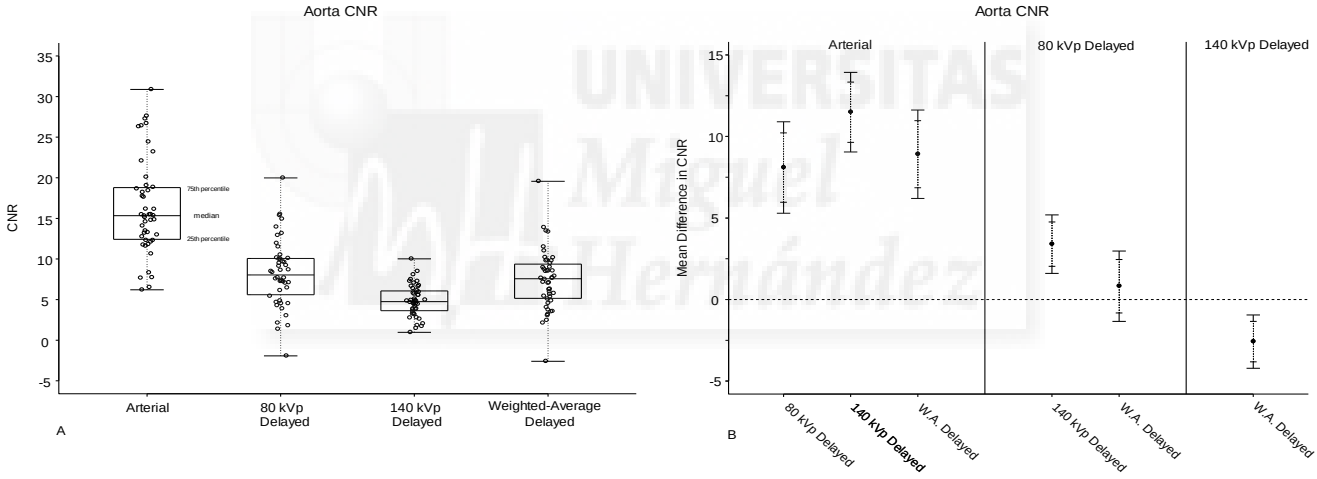

There was no difference in the endoleak CNR between arterial and 80kVp delayed images (p=0.25), nor between the arterial and the WA (p=0.134). Between the different delayed datasets, the endoleak CNR in 80kVp was not significantly different from the WA (p=0.96) (Fig.6). At 80kVp the endoleak attenuation and the image noise were significantly higher when compared with WA images (p<0.001 for both of them) (Table 2).

Fig 6.— Endoleak CNR comparison between different phases and photon energy levels. A) Box and whisker plot of the distributions of the endoleak CNR measurements under the different phase and photon energy levels. B) 95% confidence intervals for the mean differences in endoleak CNR between the different phases and photon energy levels. Note that the confidence interval furthest to the left is for the difference between the mean arterial phase CNR and mean 80 kVp delayed CNR and the confidence interval furthest to the right is for the difference between the mean l40 kVp delayed phase CNR and the mean WA delayed CNR. Also note that the dotted vertical segment of the confidence interval denotes the 95% confidence interval when the length of the interval is not adjusted for multiple comparisons, while the combined length of the dotted and solid vertical segment of the confidence interval denotes the 95% confidence interval when the length of the interval is adjusted for a total of 6 paired comparisons.

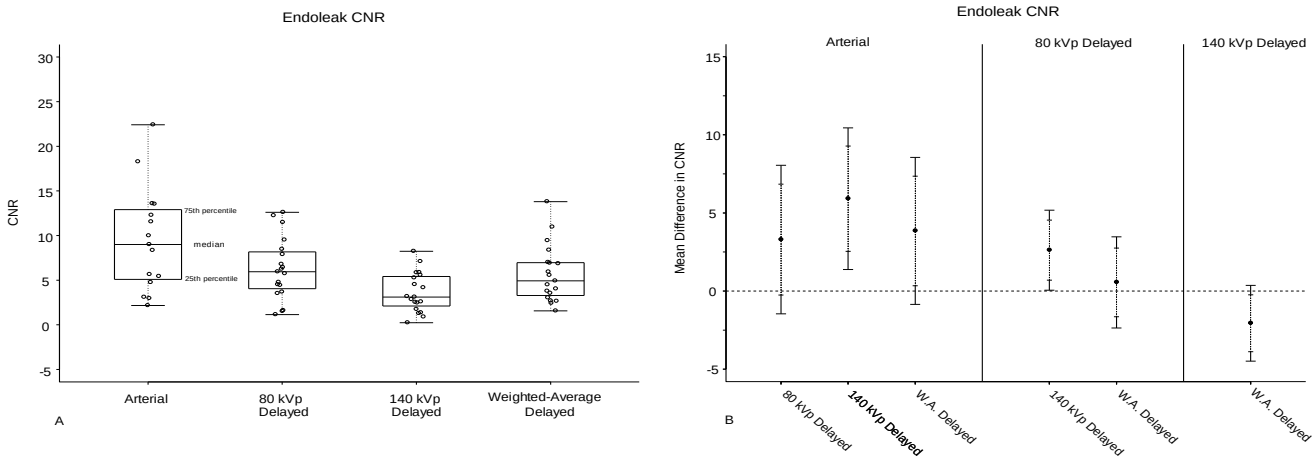

Radiation Doses

The calculated mean ED was: 4.5±2.1mSv (range, 1.8-11.6) for standard noncontrast, 13±4mSv (range, 5-21.8) for arterial phase, and 4.3± 1.9mSv (range, 1.9-11.4) for DE delayed phase. Note that the mean dose of the SECT arterial phase was greater than it was for the other acquisitions due to the expanded scan length of this phase. The mean total ED was 22.4±6.5mSv (range, 11.8-38.4). The elimination of the true noncontrast acquisition resulted in an average radiation dose reduction of 19.5% (range 10.2%- 32.8%).

The area of coverage of the nonenhanced and delayed phases was limited to the stent graft in our current protocol. To determine the reduction in radiation exposure obtained with a single DE delayed-phase acquisition relative to the triple–phase acquisition, we calculated the ED of a delayed scan with identical scan length as the arterial acquisition by multiplying the CTDI of the delayed scan

with the scan range of the arterial scan. The resulting DLP's were then multiplied with the conversion factor as described above. The calculated mean ED was: 9.8 ±3.2mSv (range, 3.4-17). Elimination of the true noncontrast and the arterial acquisitions resulted in an average radiation dose reduction of 64.1% (range 51.7%- 83.4%).

5.2.Resultados del segundo artículo en que se basa esta tesis doctoral: Imaging Follow-up of Endovascular Repair of Type B Aortic Dissection with Dual-Source, Dual-Energy CT and Late Delayed-Phase Scans. Flors L, Leiva-Salinas C, Norton PT, Patrie JT, Hagspiel KD. Vasc Interv Radiol. 2014 Mar;25(3):435-42.

24 patients (16 men; mean age, 61years; range, 26-87 years) underwent 53 triple-phase CT examinations. Average time interval between TEVAR and CT was 286 days (range, 1-1249 days).

Reading Session A

Session A, considered the reference standard, revealed 37 endoleaks in 30 of the 53 studies (56.6%). The endoleaks were diagnosed in 14 of the 24 patients (58.3%), and were classified as type IA in 8 cases (21.6%), and type II in 29 cases (78.4%). Twenty-five of the type II endoleaks (86.2%) were caused by retrograde flow through intercostal arteries and 4 (13.8%) through bronchial arteries. Type III and IV endoleaks were not depicted. Six endoleaks (16.2%) were only depicted in the delayed phase and were classified as low-flow endoleaks.

Interobserver agreement for endoleak detection in this session was high (k=0.77; 95% CI: [0.60, 0.93]), with a percentage of agreement of 88.5% (95% CI: [77.8%, 95.2%]). A consensus reading was required for 7 cases.

The patency of false lumen was graded as 1 in 4 cases (7.6%), 2 in 5 (9.4%), 3 in 24 (45.3%), 4 in 14 (26.4%) and 5 in 6 (11.3%).

Reading Session B

Session B correctly depicted 31 of the 37 endoleaks (83.8%). The endoleaks were diagnosed in 12 of the 24 patients (50%) and were classified as type IA in 8 cases (25.8%) and type II in 23 (74.2%). Type III and IV endoleaks were not depicted. Interobserver agreement for endoleak detection in this session was excellent (k=0.93; 95% CI:[0.84, 1.00]), with a percentage of agreement of 96.7% (95% CI: [88.5%, 99.6%]). A consensus reading was required for one case.

Six patients had false-negative (FN) image interpretations. All of them were low-flow type II endoleaks caused by retrograde flow through intercostal arteries which were not possible to depict in absence of the delayed phase (Fig.1). There was one false positive (FP) case of type B endoleak (Fig.2) resulting from incorrect iodine removal of residual contrast from a recent aortogram on the virtual noncontrast.

Fig 1.— Reading Session B False Negative Case. 83-year old male with low-flow type II endoleak arising from a bronchial artery in follow-up CT 96 days after TEVAR for type B aortic dissection. Standard nonenhanced (a), virtual noncontrast (b), arterial phase (c) and DE WA delayed phase (d). Presence of contrast within the aneurysm sac beyond the graft (arrows) is correctly depicted

on the 300-seconds late-delayed phase (d) representing a slow-flow endoleak not present on the arterial phase (c).

Fig 2.— Reading Session B and C False Positive Case. 71-year old male, follow-up CT 779 days after TEVAR for type B aortic dissection. The patient underwent an embolization of a type II endoleak the previous day. Standard nonenhanced (a), virtual non contrast (VNC) (b), arterial phase (c) and DE WA delayed phase (d) images are shown. Presence of contrast material within the aneurysm sac beyond the graft (arrow) is present on both arterial (c) and delayed

phase (d). There is absence of high attenuation material in the corresponding location on VNC (b) and it was incorrectly diagnosed as a type II endoleak. Standard unenhanced image (a) reveals the presence of contrast material in the same location indicating residual contrast from the recent aortogram (arrow).

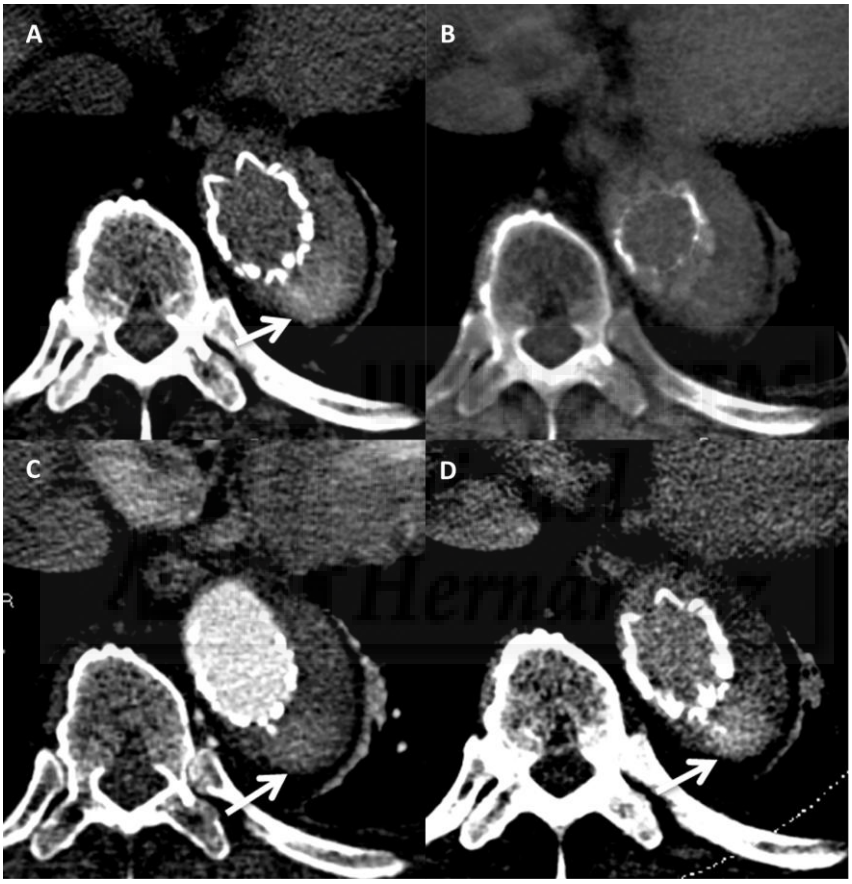

The diagnostic performance of reading session B regarding the endoleak detection, as compared with session A is represented in table 1. Agreement between reading session A and B was high (k=0.77; 95% CI: [0.61, 0.93]). No significant discordance in endoleak detection accuracy was found between session B and A (p=0.125).

Table 1. Diagnostic Performance regarding Endoleak Detection of Reading Session B and C as Compared to the Reference Standard (Session A)

Reading Session	Absolute agreement	Sensitivity	Specificity	NPV	PPV
B	88.5% (95% CI: [77.8%, 95.3%])	83.8% (95% CI: [68%, 93.8%])	95.8% (95% CI: [78.9%, 99.9%])	79.3% (95% CI: [60.3%, 92%])	96.9% (95% CI: [83.8%, 99.9%])
C	88.4% (95% CI: [77.8%, 95.3%])	100% (95% CI: [90.5%, 100%])	95.8% (95% CI: [78.9%, 99.9%])	100% (95% CI: [85.2%, 100%])	97.4% (95% CI: [86.2%, 99.9%])
NPV= Negative Predictive Value PPV= Positive Predictive Value					

The patency of false lumen was graded as 2 in 6 (11.3%), 3 in 27 (51%), 4 in 14 (26.4%) and 5 in 6 (11.3%). The percentage of agreement between reading session B and A, regarding the patency of the false lumen was 86.8% (95% CI: [74.6%, 94.5%]).

Reading Session C

Session C correctly depicted all 37 endoleaks (100%). The endoleaks were correctly classified as type IA in 8 cases (21.6%), and type II in 29 cases (78.4%). Interobserver agreement for endoleak detection in this session was excellent (k=0.93; 95% CI: [0.84, 1.00]), with a percentage of agreement of 96.7% (95%

CI: [84%, 100%]). A consensus reading was required for two cases. There was one FP case (the same as session B) related to incorrect iodine removal on the virtual noncontrast images (Fig.2). There were no false-negative (FN) image interpretations.

The diagnostic performance of reading session C, as compared with session A is shown in Table 1. There was excellent agreement between reading session C and A regarding the presence or absence of endoleak (k=0.96; 95% CI: [0.90, 1.00). No significant discordance in endoleak detection accuracy was found between session C and A (p=1.00).

There was perfect agreement regarding the assessment of false lumen patency between reading session C and A (95% CI: [93.1%, 100%]). The level of the agreement between the patency scores of session B and session A was significantly less when compared to reading session C vs. session A, (p=0.013) (Fig.3).

Fig 3.— Underestimation of patency of false lumen. 61-year old female, follow-up CT 923 days after TEVAR for type B aortic dissection. Arterial phase (a,b) and late-delayed phase (c,d). Partial patency of the false lumen was graded as <50% on the arterial phase images (a,b), whereas it was found to be >50% on the delayed phase (c,d).

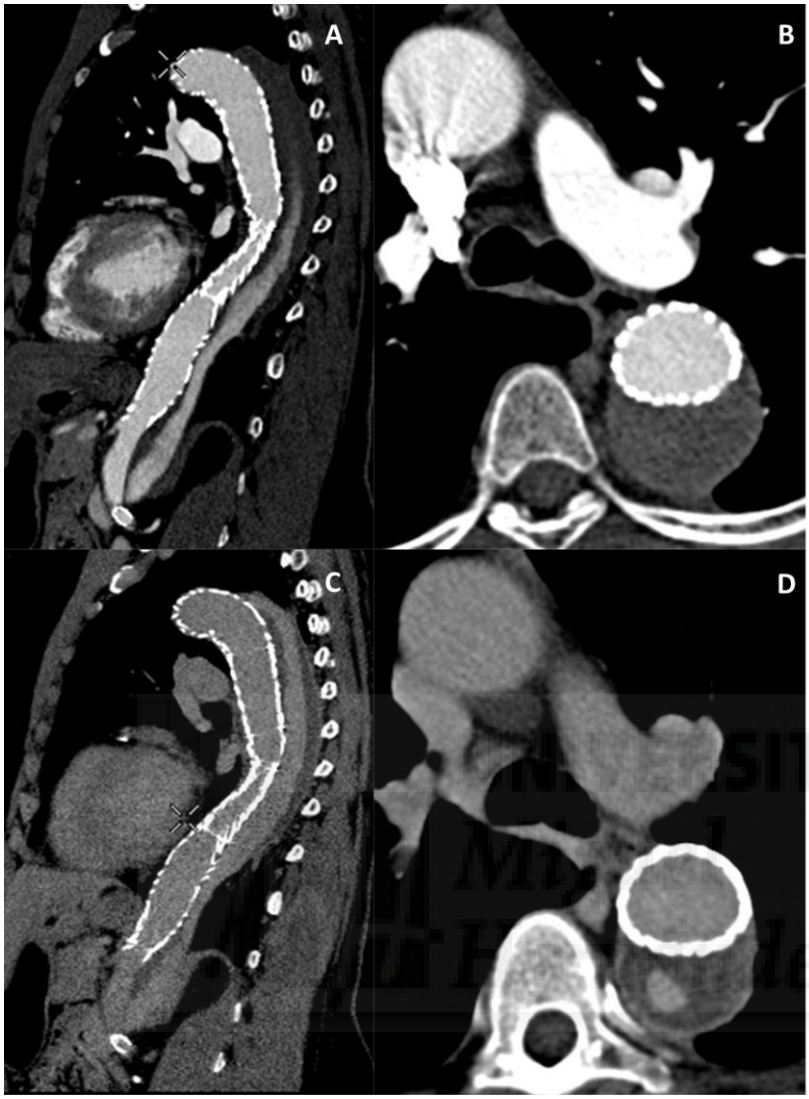

Radiation Doses

The mean total ED for the standard triple phase protocol was 23.6±8.9mSv (range, 8.8-42.2). The mean ED calculated for each acquisition was: 3.9±1.9mSv (range, 1.2-9.4) for standard unenhanced, 14.8±6.3mSv (range, 5.1-29.7) for arterial phase and 3.9±1.5mSv (range, 1.4-9.5) for DE delayed phase. The elimination of the standard unenhanced acquisition resulted in an average radiation dose reduction of 17% (range 7.7%- 29.8%); the elimination of the

unenhanced and delayed acquisition resulted in dose reduction of 21% (range, 9.6-42.5).

DISCUSIÓN

6. DISCUSIÓN

6.1. DISCUSIÓN DEL PRIMER ARTÍCULO EN QUE SE BASA ESTA TESIS DOCTORAL:

Endoleak detection after endovascular repair of thoracic aortic aneurysm using dual-source dual-energy CT: suitable scanning protocols and potential radiation dose reduction. Flors L, Leiva-Salinas C, Norton PT, Patrie JT, Hagspiel KD. AJR Am J Roentgenol. 2013;200(2):451-60.

The main advantage of DECT is the ability to differentiate and characterize different materials within the body by their different absorptiometric characteristics at low and high photon energy [11,12]. Material-specific images datasets, like VNC images, can be derived mathematically from the simultaneous availability of attenuation measurements at 2 energy levels.

One of the most valuable tools of DECT for the imaging follow-up after EVAR is the capability to obtain VNC images. These obviate the need to obtain standard nonenhanced images and thus reduce radiation dose. The results of our study demonstrate that VNC CT images reconstructed from a contrast-enhanced DECT acquisition can replace the standard nonenhanced images.

Furthermore, the accuracies for endoleak detection using either a single-phase DE CT acquisition obtained 5 minutes after the contrast material injection (LD phase) or a double-phase acquisition using arterial and DECT LD phases were not significantly different from that of the standard triple-phase CT protocol,

with a sensitivity of 85.7% and 100% respectively and a specificity of 100% in both. The interobserver agreement in the endoleak detection was excellent by using the triple phase CT protocol, and remained high with the single and double-phase protocols. While the confidence level in endoleak diagnosis was high in 94.6% of the cases when the arterial images were available, it decreased to 86.5% when only the delayed images were used; however, this difference was not statistically significant.

It has been shown previously that a delayed phase scan can demonstrate slow flow endoleaks that are not visualized during the arterial phase [5-7]. Less clear is the optimal scan delay for the delayed phase images. Many centers use a delay of 60 – 100 seconds, but one previous study reported a delayed phase scan at 300 seconds to be superior for the detection of low-flow endoleaks [9], which led us to adopt this scan delay at our institution. 19% of the endoleaks in our study were not seen on the arterial phase scan and were therefore classified as low-flow endoleaks.

In absence of an arterial phase scan it may be difficult to determine whether an endoleak is high- or low-flow in some cases. While this information is certainly desirable, this distinction does not primarily influence the management. The decision to treat mainly depends on type of endoleak and increase in aneurysm sac size. In addition, very slow flow endoleaks can escape detection if the traditional CT protocol is performed. Some patients considered having endotension (type V) endoleaks may, in fact, have very slow flow endoleaks that were not evident with a traditional scan delay. Thus the use of a LD phase can

have an impact on management, as an endoleak would be primarily treated with sac embolization rather than open surgical repair.

Two recent studies [16,17] have assessed the diagnostic performance of DECT after endovascular treatment of abdominal aortic aneurysms. In these, the DE delayed phase was performed using a 60-70 second scan delay, and it showed 100% sensitivity in endoleak detection in both studies, with 100% and 96% specificity. We missed 3 endoleaks in our study when only using the DE acquisition. However, all three were small endoleaks occupying less than 3% of the aneurysm sac who spontaneously regressed on follow-up studies. In retrospect two of the three FN cases were present even on these datasets, and they were missed mainly due to the decreased contrast between leak and thrombus in the sac compared to arterial phase.

Our cohort contains five endoleaks with less than 3% sac size. Three of these five spontaneously regressed during follow-up, one showed both decrease in leak size as well as decreased aneurysm sac size at 12 months and one was unchanged at 12 month follow-up with stable aneurysm sac size. While we don't think that it is clinically unnecessary to diagnose these, their clinical course suggests these to behave more benign. In addition, the decision when and how to treat endoleaks depends mainly on the type of leak and the presence of increased aneurysm sac size and less so on the size of the endoleak. Type I and III leaks generally require immediate treatment, regardless of size, while type II and IV endoleaks can be managed conservatively as long as the aneurysm sac does not increase in size.

In line with previous studies [7,16,17], our results show that eliminating the arterial phase does not significantly decrease diagnostic accuracy.

The DECT "three-material decomposition" algorithm usually analyzes iodine, soft tissue, and fat to obtain the VNC images. Calcium is not among these three materials, and this may result in erroneous subtraction of calcification within the aneurysm sac in the VNC when compared with the true unenhanced images, leading to potential FP diagnosis. In our study the level of calcium subtraction on the VNC images was rated on average as none to minimal and FP diagnoses were not present. Similar to previous studies [18,19], luminal aortic attenuation on VNC images showed no significant difference when compared with that on true unenhanced images, indicating sufficient removal of iodine from DECT images. None of the FN cases found in our study was due to incorrect iodine removal on the VNC images. Our qualitative and quantitative analysis of the VNC images support the hypothesis that VNC images can replace the standard nonenhanced images, and therefore, reduce the radiation dose. In addition, technological improvements on the second generation dual-source CT scanners such as tin filtration have further improved the image quality of VNC images.

Because there is increased photoelectric interaction at lower kilovoltage, iodinated contrast material has higher attenuation at 80kVp when compared to 140 and 120kVp. The increased iodinated vascular enhancement at low kVp may represent an additional potential advantage of DECT because the conspicuity of contrast material may be improved and small leaks be better depicted. However, the use of low kVp techniques is associated with increased image noise. In line

with previous published data [28], we found vascular attenuation and image noise to be significantly higher in the 80kVp images when compared to the WA 120kVp-equivalent images. More interestingly, the endoleak CNR was not significantly different between the arterial and the 80 kVp and WA delayed. For shorter scan delays (60 seconds) the endoleak CNR at 80kVp has been shown to be even higher than on the arterial phase scan on DECT [17].

Our qualitative evaluation of the detectability of endoleak by each LD DE datasets showed, in accordance to the CNR measurements, no differences between the 80 kVp and WA delayed images. In our experience it is sufficient to review the WA images only rather than both datasets. The WA images are also preferable due to the fact that they include the full field of view rather than the limited FOV of the B-tube.

The use of a dual-phase or a single-phase protocol resulted in a reduction in radiation exposure of 19.5% and 64.1% respectively relative to the standard triple-phase protocol; which is particularly important in patients after EVAR that undergo lifelong imaging surveillance with multiphase acquisitions. Our results are in line with previous studies for abdominal aortic EVAR which have demonstrated an average dose reduction for DECT of about 61% when compared with the triple-phase protocol [16,17] and 40% when compared with a dual-phase protocol [16,19]. The smaller dose savings for the dual-phase acquisition found in our study is related to the fact that the unenhanced scan in our protocol is limited to the length of the stent.

There are some limitations in our study. Type I, III, and IV endoleaks were

not present in our patient population, so the diagnostic performance of LD DECT in their diagnosis was not evaluated. It is possible that particularly type I and III endoleaks, which directly arise from the aorta, are better visualized during an earlier phase. We did not compare early and LD phases, and therefore could not assess if a LD phase, performed at 300 seconds, is truly superior to scan delays of 60 – 100 sec for the detection of slow flow endoleaks, as suggested by Iezzi *et al.*[9]. Due to the limited number of patients, it is possible that the reviewers had recognized individual cases from the previous readings even having analyzed them randomly.

One of the known limitations of VNC images is the possibility of a FP diagnosis of endoleak related to DE-based removal of iodine trapped in the aneurysm sac in the early postprocedural period [16]. Although early follow-up examinations after TEVAR were included in our study, none of them had residual contrast material in the aneurysm. Therefore we would caution to obtain a standard unenhanced acquisition during the early follow-up examinations. Another potential limitation inherent to our DECT technique is the fact that the B-tube (the tube scanning at 80kVp) in the first-generation dual-source DECT system used in our study has a FOV limited to a diameter of 26.8 cm. Careful positioning of the patient on the table and the object of interest in the center of the gantry helps minimize this limitation, and indeed in no case in our study incomplete coverage of the target affected endoleak detection. Furthermore, this has been improved on the second-generation dual-source scanners that provide a 33 cm FOV for the B tube.

In conclusion, VNC and LD phase images reconstructed from a single contrast-enhanced DECT acquisition can replace the standard triple-phase protocol in follow-up examinations after TEVAR, providing a significant dose reduction.

6.2. DISCUSIÓN DEL SEGUNDO ARTÍCULO EN QUE SE BASA ESTA TESIS DOCTORAL:

Imaging Follow-up of Endovascular Repair of Type B Aortic Dissection with Dual-Source, Dual-Energy CT and Late Delayed-Phase Scans. Flors L, Leiva-Salinas C, Norton PT, Patrie JT, Hagspiel KD. Vasc Interv Radiol. 2014 Mar;25(3):435-42.

Our results demonstrate that virtual noncontrast images can replace standard nonenhanced images after TEVAR for type B aortic dissections with an average radiation dose reduction of 17 %. This is especially relevant in this patient cohort because of the need for lifelong imaging follow-up. Our results are similar to previous studies assessing the value of virtual noncontrast images after endovascular repair of abdominal aortic aneurysm, which have demonstrated an average dose reduction of about 40% [10,12]. We found less dose saving because our unenhanced phase was limited to the stent length, whereas the whole chest was covered on these studies. A 19% dose reduction has been reported when using a similar approach for imaging follow-up after TEVAR of aortic aneurysms (8).

In our study, the accuracy in endoleak detection of a single-phase or a double-phase CT acquisition were not significantly different from that of the standard triple-phase protocol. However, the double-phase performed better (k=0.96 vs k=0.77) because it was able to depict low-flow endoleaks missed on the arterial phase. These results are similar to previous studies [5-7], some of them

using DECT [10,11], which demonstrated the value of a delayed phase in low-flow endoleak depiction. The optimal scan delay for the delayed phase scan has not been established. Although 60 –100 seconds is the most frequently adopted, we use a delay of 300 seconds at our institution based on our own experience and a study which showed that this phase was superior for the detection of very low-flow endoleaks [4]. 16.2% of the endoleaks in our study were not seen on the arterial phase scan and were therefore classified as low-flow endoleaks.

TEVAR has emerged as a treatment option in the management of type B aortic dissection with low periprocedural mortality and morbidity [1]. It aims to cover the primary entry tear to restore normal blood flow in the true lumen and induce thrombosis of the false lumen [2]. Nonclotting of the false lumen is a predictor of a poor prognosis [2,3], therefore, correct assessment of its patency is paramount. We found that without the delayed phase the patency of false lumen was significantly underestimated. Several studies have investigated the long-term changes in false lumen size and perfusion after TEVAR [17-19] but the scanning protocol used was not specifically stated.

The capability of DE CT in the imaging follow-up after endovascular repair of aortic aneurysms has been studied [8,10-13]. To the best of our knowledge neither the role of DE CT nor the value of a LD phase have been reported for TEVAR for type B aortic dissections. With such an approach, we sought to obtain an optimal protocol for complete assessment of both the true and false lumen and endoleaks, including slow-flow endoleaks, with minimal radiation dose. We believe we have achieved these objectives with our protocol.

Incorrect removal of iodine retained in the aneurysm sac in the early post-procedural period is one of the known limitations of replacing true non-contrast images with virtual noncontrast [10], as it can result false positive endoleak diagnoses. This occurred in one of our patients who was scanned the day after an embolization and had residual contrast within the false lumen. Its incorrect removal resulted in a FP when using virtual noncontrast (Fig. 2). We consider using the standard unenhanced acquisition mandatory during the early post-procedural period.

Our study had certain limitations. First, as stated earlier, the arterial phase was not acquired in DE mode; therefore, session B was not strictly a single-phase protocol. Although the virtual noncontrast images were not truly derived from the arterial but the delayed phase, we would not expect a different outcome had the arterial phase scan be performed in the DE mode, based on the iodine subtraction principle and our own extensive experience with DE CT imaging. Second, we did not compare our LD phase (300 sec) with the standard delayed phase (60 – 100 sec) to be able to assess the expected superiority of the LD phase in the detection of slow-flow endoleaks, as suggested by Iezzi *et al* [4], or in the assessment of the false lumen patency. Third, the number of patients included in our study was small and it is possible that the reviewers recognized specific cases from the previous readings despite blinded review in random order and a time interval between sessions.

In conclusion, DE CT virtual noncontrast images can replace the standard unenhanced images in follow-up examinations after endovascular repair of type B

aortic dissection and, therefore, DE CT allows to reduce radiation dose. A LD phase is valuable in the detection of slow-flow endoleaks and the correct assessment of the patency of false lumen.

UNIVERSITAS
Miguel
Hernández

CONCLUSIONES

7. CONCLUSIONES6. DISCUSIÓN

7.1. CONCLUSIÓN DEL PRIMER ARTÍCULO EN QUE SE BASA ESTA TESIS DOCTORAL: Endoleak detection after endovascular repair of thoracic aortic aneurysm using dual-source dual-energy CT: suitable scanning protocols and potential radiation dose reduction. Flors L, Leiva-Salinas C, Norton PT, Patrie JT, Hagspiel KD. AJR Am J Roentgenol. 2013;200(2):451-60.

VNC and LD phase images reconstructed from a single contrast-enhanced DECT acquisition can replace the standard triple-phase protocol in follow-up examinations after TEVAR, providing a significant dose reduction.

7.2. CONCLUSIÓN DEL SEGUNDO ARTÍCULO EN QUE SE BASA ESTA TESIS DOCTORAL: Imaging Follow-up of Endovascular Repair of Type B Aortic Dissection with Dual-Source, Dual-Energy CT and Late Delayed-Phase Scans. Flors L, Leiva-Salinas C, Norton PT, Patrie JT, Hagspiel KD. Vasc Interv Radiol. 2014 Mar;25(3):435-42.

DE CT virtual noncontrast images can replace the standard unenhanced images in follow-up examinations after endovascular repair of type B aortic dissection and, therefore, DE CT allows to reduce radiation dose. A LD phase is

valuable in the detection of slow-flow endoleaks and the correct assessment of the patency of false lumen.

BIBLIOGRAFÍA

8.1. BIBLIOGRAFÍA DE LA INTRODUCCIÓN

1. Frush KS, Alton M, Frush DP. Development and implementation of a hospital-based patient safety program. *Pediatr Radiol* 2006; 36:291-298

2. Kohn KT, Corrigan JM, Donaldson MS (1999). To err is human: building a safer health system. National Academy Press

3.Thrall JH. Quality and safety revolution in health care. *Radiology* 2004; 233:3-6

4.Donnelly LF, Dickerson JM, Goodfriend MA, Muething SE. Improving patient safety in radiology. *AJR Am J Roentgenol* 2010; 194:1183-1187

5.Johnson CD, Miranda R, Osborn HH, et al. Designing a safer radiology department. *AJR Am J Roentgenol* 2012; 198:398-404

6.Kruskal JB, Anderson S, Yam CS, Sosna J. Strategies for establishing a comprehensive quality and performance improvement program in a radiology department. *Radiographics* 2009; 29:315-329

7.Hillman BJ, Amis ES,Jr, Neiman HL, FORUM Participants. The future quality and safety of medical imaging: proceedings of the third annual ACR FORUM. *J Am Coll Radiol* 2004; 1:33-39

8.Rubin DL. Informatics in radiology: Measuring and improving quality in radiology: meeting the challenge with informatics. *Radiographics* 2011; 31:1511-1527

9.Amis ES,Jr, Butler PF, Applegate KE, et al. American College of Radiology white paper on radiation dose in medicine. *J Am Coll Radiol* 2007; 4:272-284

10.Mettler FA,Jr, Briggs JE, Carchman R, Altobelli KK, Hart BL, Kelsey CA. Use of radiology in U.S. general short-term hospitals: 1980-1990. *Radiology* 1993; 189:377-380

11.Picano E. Sustainability of medical imaging. Education and debate. *BMJ* 2004; 578-580

12.Mettler FA,Jr, Bhargavan M, Faulkner K, et al. Radiologic and nuclear medicine studies in the United States and worldwide: frequency, radiation dose, and comparison with other radiation sources--1950-2007. *Radiology* 2009; 253:520-531

13.Picano E, Vano E, Rehani MM, et al. The appropriate and justified use of medical radiation in cardiovascular imaging: a position document of the ESC Associations of Cardiovascular Imaging, Percutaneous Cardiovascular Interventions and Electrophysiology. *Eur Heart J* 2014; 35:665-672

14.World Health Organization, International Agency for Research on Cancer. Overall evaluations of carcinogenicity to humans, list of all agents evaluated to date. 2014.

15.Pierce DA, Preston DL. Radiation-related cancer risks at low doses among atomic bomb survivors. *Radiat Res* 2000; 154:178-186

16.Regulla DF, Eder H. Patient exposure in medical X-ray imaging in Europe. *Radiat Prot Dosimetry* 2005; 114:11-25

17.International Commission on Radiological Protection. ICRPpublication 87: managing patient dose in computed tomography. A report of the International Commission on Radiological Protection. Ann ICRP 2000; 30:7-45.

18.Berrington de Gonzalez A, Darby S. Risk of cancer from diagnostic X-rays: estimates for the UK and 14 other countries. *Lancet* 2004; 363:345-351

19. National Research Council. Health risks from exposure to low levels of ionizing radiation. BEIR VII Phase 2. Washington, DC: National Academies Press; 2006.

20.Annex D. Exposures from the Chernobyl accident. Available at: http:// www.unscear.org/docs/reports/1988annexd.pdf.

21.Smith-Bindman R, Lipson J, Marcus R, et al. Radiation dose associated with common computed tomography examinations and the associated lifetime attributable risk of cancer. *Arch Intern Med* 2009; 169:2078-2086

22.Durand D, Mahesh M. Understanding the CT Dose Display. *Journal of the American College of Radiology* 2012; 9:669–671

23.Bongartz G, Golding S, Jurik A, Leonardi M, van Meerten E, Rodríguez R. European Guidelines for Multislice Computed Tomography. 2004; Contract number FIGM-CT2000-20078-CT-TIP:

24.Huda W, Ogden KM, Khorasani MR. Converting dose-length product to effective dose at CT. *Radiology* 2008; 248:995-1003

25.McCollough CH, Bruesewitz MR, Kofler JM,Jr. CT dose reduction and dose management tools: overview of available options. *Radiographics* 2006; 26:503-512

26.Goodman T. Ionizing radiation effects and their risk to humans. *Image Wisely Radiation Safety in Adult Medical Imaging* 2010;

27.Stewart FA, Akleyev AV, Hauer-Jensen M, Hendry JH, Kleiman NJ, Macvittie TJ,Aleman BM, Edgar AB, Mabuchi K, Muirhead CR, Shore RE, Wallace WH. ICRP statement on tissue reactions and early and late effects of radiation in normal tissues and organs—threshold doses for tissue reactions in a radiation protection context. Ann ICRP 2012;41:1-322.

28.Rehani MM, Vano E, Ciraj-Bjelac O, Kleiman NJ. Radiation and cataract. *Radiat Prot Dosimetry* 2011; 147:300-304

29.UNSCEAR 2008 Report: Sources and effects of ionizing radiation . Vol. I. Available at: http://www.unscear.org/docs/reports/2008/09-86753_Report_2008_Annex_A.pdf.

30.The 2007 recommendations of the International Commission on Radiological Protection. ICRP Publication 103.2007;37:1-34.

31.Einstein AJ, Weiner SD, Bernheim A, et al. Multiple testing, cumulative radiation dose, and clinical indications in patients undergoing myocardial perfusion imaging. *JAMA* 2010; 304:2137-2144

32. McCollough CH, Primak AN, Braun N, Kofler J, Yu L, Christner J. Strategies for reducing radiation dose in CT. *Radiol Clin North Am* 2009; 47:27-40

33.Johnson TR, Krauss B, Sedlmair M, et al. Material differentiation by dual energy CT: initial experience. *Eur Radiol* 2007; 17:1510-1517

34.Remy-Jardin M, Faivre JB, Pontana F, et al. Thoracic applications of dual energy. *Radiol Clin North Am* 2010; 48:193-205

35.Vlahos I, Godoy MC, Naidich DP. Dual-energy computed tomography imaging of the aorta. *J Thorac Imaging* 2010; 25:289-300

8.2. BIBLIOGRAFÍA ESPECÍFICA

8.2.1. Bibliografía del primer artículo en que se basa esta tesis doctoral:

Endoleak detection after endovascular repair of thoracic aortic aneurysm using dual-source dual-energy CT: suitable scanning protocols and potential radiation dose reduction. Flors L, Leiva-Salinas C, Norton PT, Patrie JT, Hagspiel KD. AJR Am J Roentgenol. 2013;200(2):451-60.

1. Baril DT, Silverberg D, Ellozy SH, et al. Endovascular stent-graft repair of failed endovascular abdominal aortic aneurysm repair. *Ann Vasc Surg* 2008; 22(1):30-36.

2. Torsello G, Osada N, Florek HJ, et al. Long-term outcome after Talent endograft implantation for aneurysms of the abdominal aorta: a multicenter retrospective study. *J Vasc Surg* 2006; 43(2):277-84.

3. Bley TA, Chase PJ, Reeder SB, et al. Endovascular abdominal aortic aneurysm repair: nonenhanced volumetric CT for follow-up. *Radiology* 2009; 253(1):253-262.

4. Stavropoulos SW, Charagundla SR. Imaging techniques for detection and management of endoleaks after endovascular aortic aneurysm repair. *Radiology* 2007; 243(3):641-655.

5. Rozenblit AM, Patlas M, Rosenbaum AT, et al. Detection of endoleaks after endovascular repair of abdominal aortic aneurysm: value of unenhanced and delayed helical CT acquisitions. *Radiology* 2003; 227(2):426-433.

6. Golzarian J, Dussaussois L, Abada HT, et al. Helical CT of aorta after endoluminal stent-graft therapy: value of biphasic acquisition. *AJR* 1998; 171(2):329-331.

7. Macari M, Chandarana H, Schmidt B, Lee J, Lamparello P, Babb J. Abdominal aortic aneurysm: can the arterial phase at CT evaluation after endovascular repair be eliminated to reduce radiation dose? *Radiology* 2006; 241(3):908-914.

8. May J, White GH, Harris JP. Endoluminal repair of abdominal aortic aneurysms - state of the art. *Eur J Radiol* 2001; 39(1):16-21.

9. Iezzi R, Cotroneo AR, Filippone A, Santoro M, Basilico R, Storto ML. Multidetector-row computed tomography angiography in abdominal aortic aneurysm treated with endovascular repair: evaluation of optimal timing of delayed phase imaging for the detection of low-flow endoleaks. *J Comput Assist Tomogr* 2008; 32(4):609-615.

10. Iezzi R, Cotroneo AR, Filippone A, et al. Multidetector CT in abdominal aortic aneurysm treated with endovascular repair: are unenhanced and delayed phase enhanced images effective for endoleak detection? *Radiology* 2006; 241(3):915-921.

11. Johnson TR, Krauss B, Sedlmair M, et al. Material differentiation by dual energy CT: initial experience. *Eur Radiol* 2007; 17(6):1510-1517.

12. Remy-Jardin M, Faivre JB, Pontana F, et al. Thoracic applications of dual energy. *Radiol Clin North Am* 2010; 48(1):193-205.

13. Vlahos I, Godoy MC, Naidich DP. Dual-energy computed tomography imaging of the aorta. *J Thorac Imaging* 2010; 25(4):289-300.

14. Godoy MC, Naidich DP, Marchiori E, et al. Single-acquisition dual-energy multidetector computed tomography: analysis of vascular enhancement and postprocessing techniques for evaluating the thoracic aorta. *J Comput Assist Tomogr* 2010; 34(5):670-677.

15. Behrendt FF, Schmidt B, Plumhans C, et al. Image fusion in dual energy computed tomography: effect on contrast enhancement, signal-to-noise ratio and image quality in computed tomography angiography. *Invest Radiol* 2009; 44(1):1-6.

16. Stolzmann P, Frauenfelder T, Pfammatter T, et al. Endoleaks after endovascular abdominal aortic aneurysm repair: detection with dual-energy dual-source CT. *Radiology* 2008; 249(2):682-691.

17. Chandarana H, Godoy MC, Vlahos I, et al. Abdominal aorta: evaluation with dual-source dual-energy multidetector CT after endovascular repair of aneurysms--initial observations. *Radiology* 2008; 249(2):692-700.

18. Numburi UD, Schoenhagen P, Flamm SD, et al. Feasibility of dual-energy CT in the arterial phase: Imaging after endovascular aortic repair. *AJR* 2010; 195(2):486-493

19. Sommer WH, Graser A, Becker CR, et al. Image quality of virtual noncontrast images derived from dual-energy CT angiography after endovascular aneurysm repair. *J Vasc Interv Radiol* 2010; 21(3):315-321.

20. White GH, Yu W, May J, Chaufour X, Stephen MS. Endoleak as a complication of endoluminal grafting of abdominal aortic aneurysms:

classification, incidence, diagnosis, and management. *J Endovasc Surg* 1997; 4(2):152-168.

21. White GH, May J, Petrasek P, Waugh R, Stephen M, Harris J. Endotension: an explanation for continued AAA growth after successful endoluminal repair. *J Endovasc Surg* 1999; 6(4):308-315.

22. White GH, May J, Waugh RC, Chaufour X, Yu W. Type III and type IV endoleak: toward a complete definition of blood flow in the sac after endoluminal AAA repair. *J Endovasc Surg* 1998; 5(4):305-309.

23. Pitton MB, Schweitzer H, Herber S, et al. MRI versus helical CT for endoleak detection after endovascular aneurysm repair. *AJR* 2005; 185(5):1275-1281.

24. Gilling-Smith G, Brennan J, Harris P, Bakran A, Gould D, McWilliams R. Endotension after endovascular aneurysm repair: definition, classification, and strategies for surveillance and intervention. *J Endovasc Surg* 1999; 6(4):305-307.

25. Huda W, Ogden KM, Khorasani MR. Converting dose-length product to effective dose at CT. *Radiology* 2008; 248(3):995-1003.

26. Agresti A. *Categorical Data Analysis*, 2nd ed. Hoboken,NJ: John Wiley and Sons, 2002.

27. Neter J, Kutner MH, Nachtsheim CJ, Wasserman W. *Applied Linear Models*, 4th ed. Chicago, IL: IRWIN, 1996.

28. Park EA, Lee W, Kang JH, Yin YH, Chung JW, Park JH. The image quality and radiation dose of 100-kVp versus 120-kVp ECG-gated 16-slice CT coronary angiography. *Korean J Radiol* 2009; 10(3):235-243.

8.2.2.Bibliografía del segundo artículo en que se basa esta tesis doctoral: Imaging Follow-up of Endovascular Repair of Type B Aortic Dissection with Dual-Source, Dual-Energy CT and Late Delayed-Phase Scans. Flors L, Leiva-Salinas C, Norton PT, Patrie JT, Hagspiel KD. Vasc Interv Radiol. 2014 Mar;25(3):435-42.

1. Sobocinski J, Dias NV, Berger L, et al. Endograft repair of complicated acute type B aortic dissections. Eur J Vasc Endovasc Surg 2013; 45:468-474.

2. Garzon G, Fernandez-Velilla M, Marti M, Acitores I, Ybanez F, Riera L. Endovascular stent-graft treatment of thoracic aortic disease. Radiographics 2005; 25 Suppl 1:S229-44.

3. Bernard Y, Zimmermann H, Chocron S, et al. False lumen patency as a predictor of late outcome in aortic dissection. Am J Cardiol 2001; 87:1378-1382.

4. Iezzi R, Cotroneo AR, Filippone A, Santoro M, Basilico R, Storto ML. Multidetector-row computed tomography angiography in abdominal aortic aneurysm treated with endovascular repair: evaluation of optimal timing of delayed phase imaging for the detection of low-flow endoleaks. J Comput Assist Tomogr 2008; 32:609-615.

5. Rozenblit AM, Patlas M, Rosenbaum AT, et al. Detection of endoleaks after endovascular repair of abdominal aortic aneurysm: value of unenhanced and delayed helical CT acquisitions. Radiology 2003; 227:426-433.

6. Golzarian J, Dussaussois L, Abada HT, et al. Helical CT of aorta after endoluminal stent-graft therapy: value of biphasic acquisition. AJR Am J Roentgenol 1998; 171:329-331.

7. Macari M, Chandarana H, Schmidt B, Lee J, Lamparello P, Babb J. Abdominal aortic aneurysm: can the arterial phase at CT evaluation after endovascular repair be eliminated to reduce radiation dose? Radiology 2006; 241:908-914.

8. Flors L, Leiva-Salinas C, Norton PT, Patrie JT, Hagspiel KD. Endoleak detection after endovascular repair of thoracic aortic aneurysm using dual-source dual-energy CT: suitable scanning protocols and potential radiation dose reduction. AJR Am J Roentgenol 2013; 200:451-460.

9. Vlahos I, Godoy MC, Naidich DP. Dual-energy computed tomography imaging of the aorta. J Thorac Imaging 2010; 25:289-300.

10. Stolzmann P, Frauenfelder T, Pfammatter T, et al. Endoleaks after endovascular abdominal aortic aneurysm repair: detection with dual-energy dual-source CT. Radiology 2008; 249:682-691.

11. Chandarana H, Godoy MC, Vlahos I, et al. Abdominal aorta: evaluation with dual-source dual-energy multidetector CT after endovascular repair of aneurysms--initial observations. Radiology 2008; 249:692-700.

12. Sommer WH, Graser A, Becker CR, et al. Image quality of virtual noncontrast images derived from dual-energy CT angiography after endovascular aneurysm repair. J Vasc Interv Radiol 2010; 21:315-321.

13. Numburi UD, Schoenhagen P, Flamm SD, et al. Feasibility of dual-energy CT in the arterial phase: Imaging after endovascular aortic repair. AJR Am J Roentgenol 2010; 195:486-493.

14. Bongartz G, Golding S, Jurik A, Leonardi M, van Meerten E. European guidelines on quality criteria for computed tomography. 2000;Publication no.

EUR 16262 EN. Luxembourg: Office for Official Publications of the European Communities;2000.

15. Bongartz G, Golding S, Jurik A, Leonardi M, van Meerten E, Rodríguez R. European Guidelines for Multislice Computed Tomography. 2004; Contract number FIGM-CT2000-20078-CT-TIP. March 2004.

16. Agresti A. Categorical Data Analysis. Second Edition ed. Hoboken,NJ: John Wiley and Sons; 2002.

17. Kusagawa H, Shimono T, Ishida M, et al. Changes in false lumen after transluminal stent-graft placement in aortic dissections: six years' experience. Circulation 2005; 111:2951-2957.

18. Schoder M, Czerny M, Cejna M, et al. Endovascular repair of acute type B aortic dissection: long-term follow-up of true and false lumen diameter changes. Ann Thorac. Surg 2007; 83:1059-1066.

19. Chemelli-Steingruber IE, Chemelli A, Strasak A, Hugl B, Hiemetzberger R, Czermak BV. Evaluation of volumetric measurements in patients with acute type B aortic dissection--thoracic endovascular aortic repair (TEVAR) vs conservative. J Vasc Surg 2009; 49:20-28.

ANEXOS

ANEXO I: CONJUNTO DE PUBLICACIONES EN LAS QUE SE BASA LA PRESENTE TESIS DOCTORAL